colony-forming units (CFU-M) as did wild-type cells, with similar rates of formation (Figures 4E and 4F). We also added G-CSF to stem cell medium and cultured bone marrow cells (Figure 4G). As expected, the colony numbers (data not shown) and morphology (Figure 4G) between the two cell types were similar, but Ly6G expression was decreased in cells derived from *Jdp2*$^{-/-}$ bone marrow colonies (Figure 4H). Together, our findings imply that the abnormality in neutrophils from *Jdp2*$^{-/-}$ mice arises in the late differentiation phase and not in the initial differentiation phase.

Finally, we determined whether reintroduction of Jdp2 could rescue the terminal differentiation. We infected *Jdp2*$^{-/-}$ bone marrow cells with a retrovirus encoding Jdp2 and GFP or GFP alone and cultured the cells in medium containing G-CSF (Figure 4I). After 9 days, the cells were harvested and their Ly6G expression levels in gated GFP-positive neutrophils were quantified by FACS (Figure 4I). As expected, *Jdp2*$^{-/-}$ bone marrow-derived neutrophils infected with the Jdp2-GFP retrovirus exhibited increased Ly6G expression compared with control GFP-only cells (Figure 4I). Thus, the defect in neutrophil differentiation in *Jdp2*$^{-/-}$ mice appears to be cell autonomous and can be corrected by re-expression of Jdp2.

Primary Granule mRNA Expression Is Elevated in *Jdp2*$^{-/-}$ Neutrophils

The mRNA levels of granule genes are higher in immature neutrophils than in mature neutrophils (Martinelli et al., 2004). Therefore, we analyzed the diverse RNAs of CD11b^{+}Ly6C^{lo}Ly6G^{+} bone marrow neutrophils encoding primary, secondary, and tertiary granules by using microarray data (Figure 5A). Intriguingly, the mRNA levels for primary granule proteins, such as MPO, CTSG, and PR3, were significantly increased in *Jdp2*$^{-/-}$ neutrophils, whereas those for secondary and tertiary granule proteins were comparable to control cells (Figure 5A). The expression of other bactericidal granule proteins, such as Lipocalin2 and Cramp, was comparable (Figure S4A). We confirmed these aberrant primary granule expressions in bone marrow and peritoneal neutrophils by qPCR (Figures 5B and 5C). However, in immunoblotting analyses, the expression levels of primary granule proteins (Figure 5D) and their degranulation in response to LPS (Figure S4B) seemed comparable between wild-type and *Jdp2*$^{-/-}$ neutrophils.

To reveal the mechanism of the aberrant mRNA expression in *Jdp2*$^{-/-}$ neutrophils, we selected a set of genes whose expression levels were more abundant in *Jdp2*$^{-/-}$ neutrophils than in wild-type cells (Figure S4C) based on microarray data and examined their promoters for the presence of transcription factor binding sites. The analysis revealed that C/EBP binding sequences were highly enriched in the promoters of Jdp2-regulated genes compared with randomly selected gene promoters (Figures S4C–S4E). Further, we found that C/EBP binding sites were most enriched among 198 transcription factor binding sequences tested (Table S1). Thus, we quantified the mRNAs of the C/EBP gene family involved in myeloid differentiation. However, their expression levels were comparable (Figure 5E). C/EBPα was reported to be the master regulator of the expression of primary granule genes (Zhang et al., 1998). Therefore, we examined the DNA-binding activities of C/EBPα and C/EBPβ to their consensus oligonucleotides by using ELISA-based transcription factor kits (Figure 5F). Although the protein expression levels were again comparable (Figure 5G), C/EBPα, but not C/EBPβ, DNA binding was increased in *Jdp2*$^{-/-}$ neutrophils (Figure 5F). In addition, Jdp2 binding to the C/EBPα promoter was not detected by chromatin immunoprecipitation (ChIP) analyses (Figure 5H). When GFP-fused Jdp2 was retrovirally overexpressed in primary neutrophils, its expression was restricted to the nucleus (Figure S4F). These observations led us to examine the binding of Jdp2 to C/EBPα, and an association between C/EBPα and Jdp2 was found by immunoprecipitation (Figures 5I and 5J). From this, we examined the effect of Jdp2 on the transcriptional activity of C/EBPα (Figure 5K). For this experiment, we used a luciferase reporter plasmid driven by C/EBP transcriptional response elements. Overexpression of the C/EBPα gene only activated this promoter, whereas simultaneous expression of Jdp2 dose dependently reduced the activity of the promoter to the control level (Figure 5K). Together, these findings suggest that Jdp2 inhibits the transcriptional activity of C/EBPα by directly binding to the gene and inhibiting C/EBPα from binding to its target sequence. We also overexpressed C/EBPα in wild-type bone marrow cells and found that C/EBPα enhanced primary granule mRNAs (Figures S4G and S4H). Furthermore, when we re-expressed Jdp2 in *Jdp2*$^{-/-}$ bone marrow cells, DNA binding of C/EBPα and expression of primary granule genes were downregulated (Figures S4I and S4J). We also overexpressed C/EBPα in wild-type differentiated neutrophils (Figure S4K) and found that expression of Bcl-2 (Figure S4M) but not Ly6G (Figure S4L) was induced, leading to impaired apoptosis (Figure S4N). Together, our observations strengthen the idea that *Jdp2*$^{-/-}$ neutrophils are immature and suggest that increased primary granule and Bcl-2 mRNA expressions are attributable to increased C/EBPα activation.

ATF3 Is a Target of Jdp2 and Regulates Ly6G Expression

Among AP-1 family members, ATF3 is the closest relative of Jdp2 (Figure 6A). This information prompted us to measure ATF3 expression in neutrophils. ATF3 expression in bone marrow and peritoneal neutrophils was significantly increased (Figure 6B). We also overexpressed Jdp2 in wild-type and *Jdp2*$^{-/-}$ neutrophils and found that Jdp2 suppressed ATF3 expression (Figures 6C and 6D). Jdp2 is known to act as an epigenetic regulator of gene expression (Jin et al., 2006). Therefore, we analyzed the genome-wide status of histone acetylation, H3K4 trimethylation, and H3K27 trimethylation in wild-type and *Jdp2*$^{-/-}$ peritoneal neutrophils by using the ChIP-sequencing (ChIP-Seq) technique (Figure 6E). First, genes were chosen based on their differences in expression in wild-type and *Jdp2*$^{-/-}$ neutrophils. However, we did not find an apparent correlation between epigenetic statuses (data not shown). Moreover, primary granule genes did not have significant peaks for acetyl-histone, H3K4me3, and H3K27me3 in either wild-type or *Jdp2*$^{-/-}$ peritoneal neutrophils (Figure S5), indicating that expression of these genes is not regulated by the epigenetic status. When we focused on the ATF3 locus, we found a dramatic increase in the acetyl-histone status of the promoter region close to the transcription start site (Figure 6E). However, the same region had comparable H3K4me3 and H3K27me3 statuses (Figure 6E). By ChIP analyses, we confirmed an increase in the acetyl-histone status at the ATF3 promoter region in *Jdp2*$^{-/-}$ peritoneal neutrophils and observed

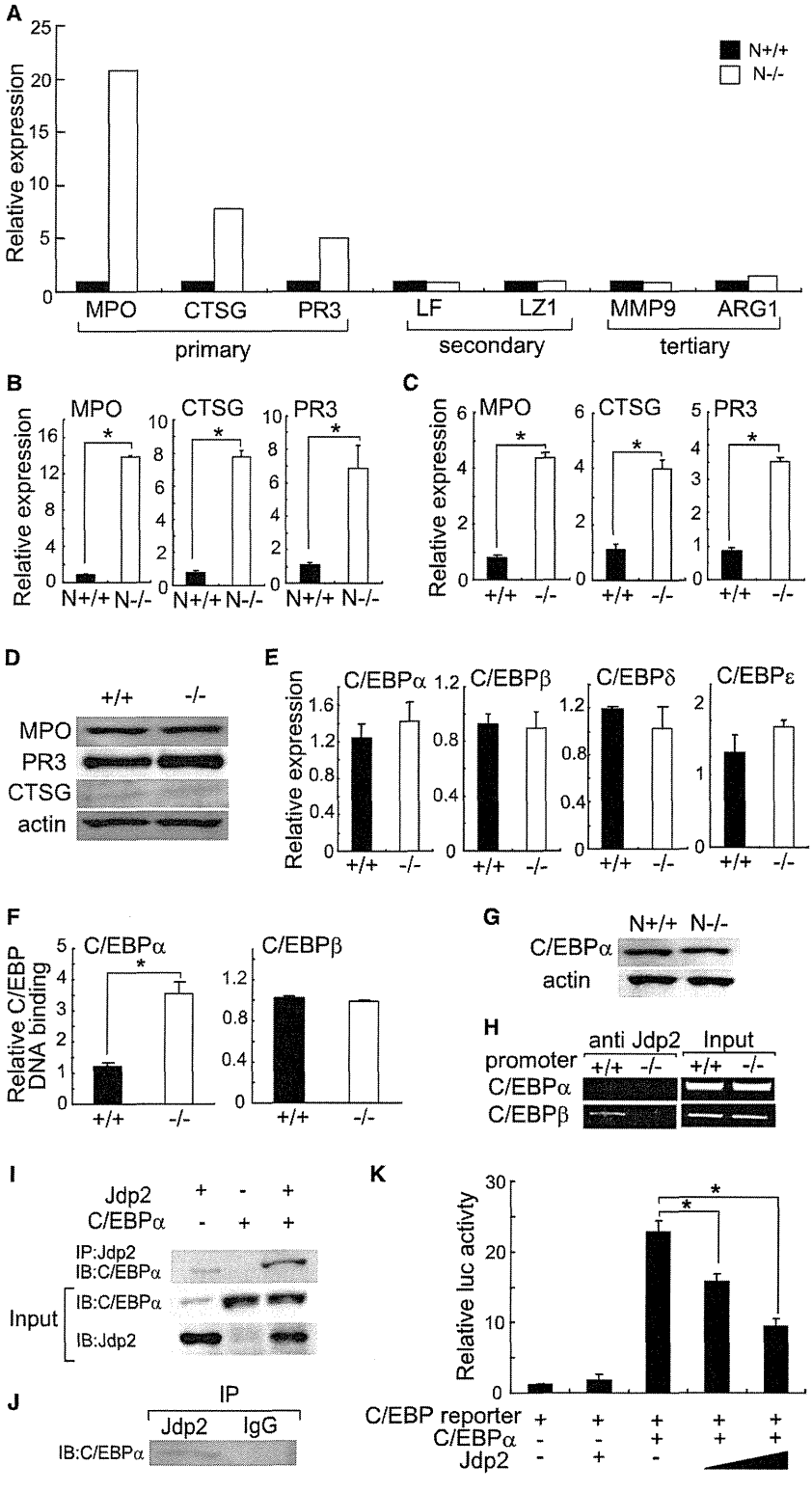

Figure 5. Aberrant mRNA Levels of Primary Granule Genes in *Jdp2*$^{-/-}$ Neutrophils

(A) Primary, secondary, and tertiary granule mRNA levels in bone marrow CD11b^{+}Ly6C^{lo}Ly6G^{+} neutrophils (N+/+ and N−/−) analyzed by a microarray.

(B and C) MPO, CTSG, and PR3 mRNA levels in CD11b^{+}Ly6C^{lo}Ly6G^{+} neutrophils (N+/+ and N−/−) (B) and peritoneal neutrophils (C) measured by qPCR.

(D) Primary granule protein levels in peritoneal neutrophils from wild-type and *Jdp2*$^{-/-}$ mice.

(E) C/EBP gene family mRNA levels in peritoneal neutrophils from wild-type and *Jdp2*$^{-/-}$ mice measured by qPCR.

(F) DNA-binding activities of C/EBPα and C/EBPβ in wild-type and *Jdp2*$^{-/-}$ peritoneal neutrophils measured with a TransAM Transcription Factor Assay Kit.

(G) C/EBPα protein levels in nuclear extracts from wild-type and *Jdp2*$^{-/-}$ peritoneal neutrophils analyzed by immunoblotting.

(H) ChIP analyses with a Jdp2 Ab of lysates from wild-type and *Jdp2*$^{-/-}$ peritoneal neutrophils. C/EBPα and C/EBPβ promoter regions were detected by PCR.

(I) 293T cells were transfected with the indicated pCMV expression vectors. After anti-Jdp2 immunoprecipitation (IP), input and immunoprecipitates were analyzed by immunoblotting with C/EBPα and Jdp2 Abs.

(J) Wild-type peritoneal neutrophils were lysed. After anti-Jdp2 and control IgG IP, immunoprecipitates were analyzed by immunoblotting with a C/EBPα Ab.

(K) Luciferase assays examining the effects of Jdp2 on the transcriptional activity of C/EBPα. Error bars, SE (n = 3). *p < 0.05.

direct binding between Jdp2 and the ATF3 promoter (Figure 6F). Furthermore, we found that Jdp2 overexpression in wild-type neutrophils suppressed ATF3 promoter acetylation (Figure 6G).

Finally, to determine whether increased ATF3 expression affected neutrophil differentiation, we infected wild-type bone marrow cells with a retrovirus encoding ATF3 and GFP or GFP alone and analyzed the cells by FACS after 5 days as described earlier. Intriguingly, neutrophils infected with the ATF3-GFP retrovirus showed decreased Ly6G expression levels but unchanged cellular morphology, compared with GFP-alone control cells (Figure 6H). Thus, ATF3 is a negative regulator of neutrophil differentiation, and its expression is strictly regulated by Jdp2.

Jdp2$^{-/-}$ Mice Are Highly Susceptible to Bacterial and Fungal Infection

Because decreased neutrophil function is an important risk factor for *C. albicans* infection, we checked the susceptibility of *Jdp2*$^{-/-}$ mice to *C. albicans* challenge (Figures 7A–7C). We observed a slight but significant increase in *C. albicans* susceptibility in *Jdp2*$^{-/-}$

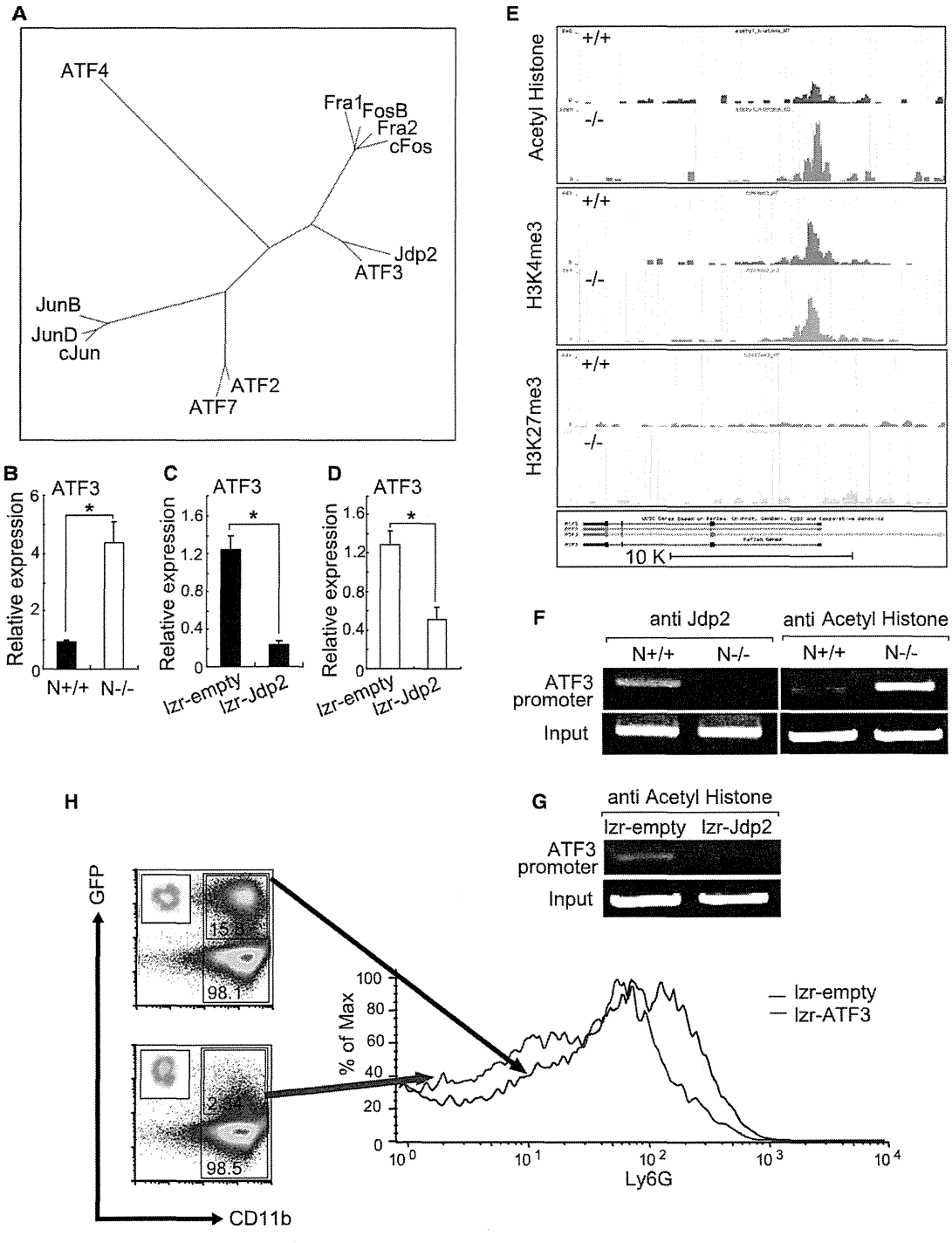

Figure 6. ATF3 Is a Target of Jdp2 and Modulates Ly6G Surface Expression

(A) Phylogenetic tree for AP-1 family proteins and Jdp2.

(B) ATF3 mRNA levels in bone marrow $CD11b^+Ly6C^{lo}Ly6G^+$ neutrophils (N+/+ and N−/−) analyzed by qPCR.

(C and D) Wild-type (C) and *Jdp2*$^{-/-}$ (D) bone marrow cells were infected with a retrovirus encoding Jdp2 and GFP (Izr-Jdp2) or GFP alone (Izr-empty) and cultured with G-CSF. After 5 days, the cells were harvested and $CD11b^+GFP^+$ cells were sorted. ATF3 mRNA levels were measured by qPCR.

(E) ChIP-seq enrichment profiles for acetyl-histone, H3K4me3, and H3K27me3 at the ATF3 locus in wild-type and *Jdp2*$^{-/-}$ peritoneal neutrophils.

(F) ChIP analyses with Jdp2 and acetyl-histone Abs of lysates from wild-type and *Jdp2*$^{-/-}$ bone marrow $CD11b^+Ly6C^{lo}Ly6G^+$ neutrophils (N+/+ and N−/−). DNA fragments of the ATF3 promoter region were detected by PCR.

(G) ChIP analyses with an acetyl-histone Ab of lysates in (C). DNA fragments of the ATF3 promoter region were detected by PCR.

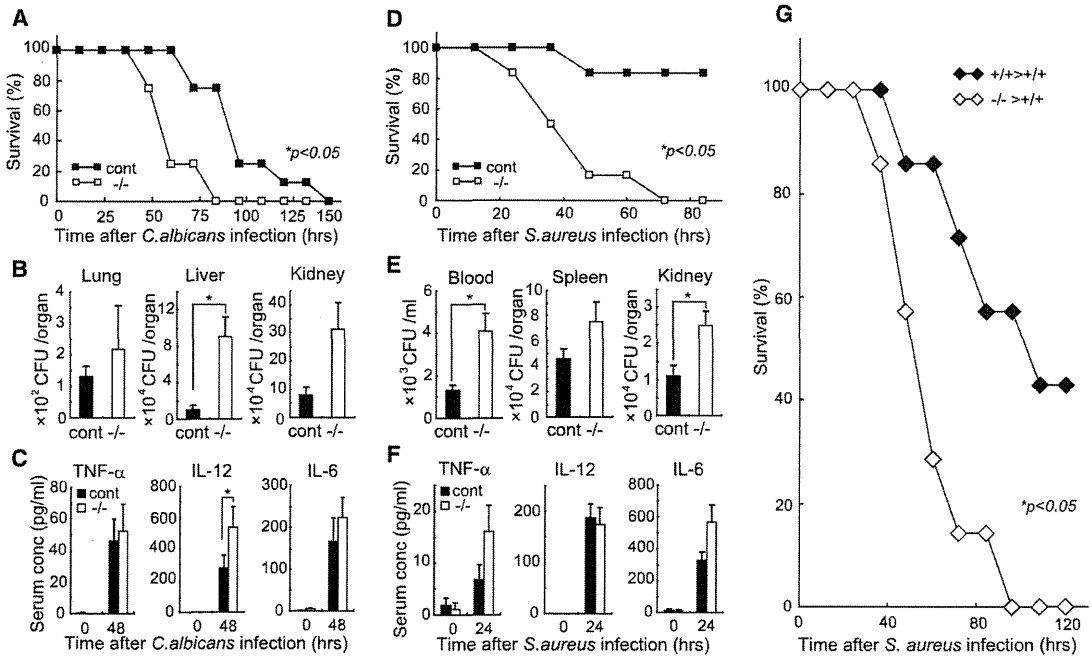

Figure 7. *Jdp2*$^{-/-}$ Mice Are Susceptible to Infection

(A–C) *C. albicans* was intravenously injected into *Jdp2*$^{+/+}$*Jdp2*$^{+/-}$ mice (control, n = 8) and *Jdp2*$^{-/-}$ mice (−/−, n = 8) and the mice were monitored (A). *Jdp2*$^{-/-}$ mice showed significantly worse survival than control mice ($p < 0.05$). CFU in the indicated organs (B) and serum cytokine levels (C) were determined at 36 hr after infection.

(D–F) *S. aureus* was intravenously injected into *Jdp2*$^{+/+}$*Jdp2*$^{+/-}$ mice (control, n = 6) and *Jdp2*$^{-/-}$ mice (−/−, n = 6) and the mice were monitored (D). *Jdp2*$^{-/-}$ mice showed significantly worse survival than control mice ($p < 0.05$). CFU in the indicated organs (E) and serum cytokine levels (F) were determined at 36 hr after infection.

(G) *S. aureus* was intravenously injected into wild-type mice reconstituted by transplantation of wild-type (+/+ > +/+, n = 7) or *Jdp2*$^{-/-}$ (−/− > +/+, n = 7) bone marrow and the mice were monitored. The survival was significantly worse in −/− > +/+ mice than in +/+ > +/+ mice ($p < 0.05$).

Error bars, SE (n = 4 unless indicated). *$p < 0.05$.

mice (Figure 7A), which showed elevated numbers of *C. albicans* CFU in their liver compared with wild-type mice (Figure 7B). The serum IL-12 levels were significantly elevated in *Jdp2*$^{-/-}$ mice, compared with wild-type mice, but the serum TNF-α and IL-6 levels were comparable (Figure 7C). We also infected *Jdp2*$^{-/-}$ and wild-type mice with *S. aureus* (Figures 7D–7F). Surprisingly, *Jdp2*$^{-/-}$ mice were highly susceptible to *S. aureus* infection, compared with wild-type mice (Figure 7D). *Jdp2*$^{-/-}$ mice showed significantly elevated numbers of *S. aureus* CFU in their blood and kidneys, compared with wild-type mice (Figure 7E). In contrast, the serum cytokine levels were not significantly altered (Figure 7F). To evaluate the relevance of hematopoietic Jdp2 deficiency to protective immunity against pathogens, we irradiated wild-type mice and reconstituted them with bone marrow from wild-type or *Jdp2*$^{-/-}$ mice (Figure 7G). Chimeric mice lacking Jdp2 in their hematopoietic system showed significantly increased susceptibility to *S. aureus* (Figure 7G). To evaluate the importance of lymphocytes in protective immunity against *S. aureus* infection in our experimental model, we depleted T and B cells in wild-type mice reconstituted with bone marrow from wild-type mice by using CD3 and CD20 Abs (Figure S6A). However, this depletion had no effect on survival in response to *S. aureus* (Figure S6B). Thus, we think our infection model reflects the function of cells other than T and B cells. Next, we depleted neutrophils in bone marrow chimeric mice by using a Ly6G Ab (Figure S6C). We infected the neutrophil-depleted chimeric mice with *S. aureus* and observed no significant difference in *S. aureus*-induced lethality between wild-type and *Jdp2*$^{-/-}$ chimeric mice (Figure S6D). Thus, these findings suggest that the increased susceptibility to *S. aureus* in *Jdp2*$^{-/-}$ mice is due to an abnormal neutrophil phenotype.

DISCUSSION

We have demonstrated that Jdp2 plays a critical role in osteoclastogenesis in vivo. We also discovered that in vitro osteoclastogenesis was completely abolished in *Jdp2*$^{-/-}$ cells. Furthermore, RANKL-mediated Jdp2 induction appeared to be

(H) Wild-type bone marrow cells were infected with a retrovirus encoding ATF3 and GFP (Izr-ATF3) or GFP alone (Izr-empty) and cultured with G-CSF. After 5 days, CD11b^{+}GFP^{+} cells were gated and Ly6G expression levels were quantified by FACS. Gated cells were also sorted and stained by May-Grunwald-Giemsa (upper left insets in the scatter plots).

Error bars, SE (n = 3). *$p < 0.05$.

regulated through c-Fos. NFATc1 activation was partially suppressed, meaning that Jdp2 may also positively regulate its activity. However, we did not detect a direct association between Jdp2 and NFATc1 (data not shown), and Jdp2 had no effect on NFATc1 binding to its promoter region. Thus, indirect mechanisms are likely to modulate the NFATc1 activity.

The defect in osteoclastogenesis in *Jdp2*$^{-/-}$ mice in vivo was relatively mild compared with its effect on in vitro osteoclastogenesis. It has been reported that calcium signaling is important for NFATc1 activation and that such costimulatory signaling is supported by ITAM-harboring adaptors, such as FcRγ and DNAX-activation protein 12 (DAP12) (Koga et al., 2004). Because RANKL-induced calcium oscillation was normal in *Jdp2*$^{-/-}$ cells in this study, signaling through ITAM-harboring molecules is likely to be normal. These findings further suggest that another unknown costimulatory signaling pathway may be compensating for the Jdp2 deficiency in vivo. Further studies are needed to explore the role of Jdp2 in osteoclasts, but our data provide insights into c-Fos-Jdp2 axis-mediated osteoclastogenesis and suggest a basis for the possibility of Jdp2-targeted therapeutic approaches to treat osteoporosis.

Our present data clearly revealed an unexpected and strict requirement for Jdp2 in proper differentiation of neutrophils. *Jdp2*$^{-/-}$ neutrophils were morphologically normal but had impaired surface expression of Ly6G, apoptosis, and bactericidal function. Furthermore, C/EBPα activation and expression of Bcl-2 and primary granule genes were increased. Our data also suggest that Jdp2 suppresses C/EBPα by directly binding to it. Notably, *Jdp2*$^{-/-}$ neutrophils showed normal primary granule protein levels but increased mRNA levels. Similar discrepancies have been reported in several knockout mice. For example, Gfi1-deficient neutrophils exhibit immature morphology and significant increases in mRNAs, such as primary granule genes and C/EBPα, but lack granules (Hock et al., 2003). Meanwhile, Ikaros-deficient neutrophils have impaired Ly6G levels but normal granule and nuclear morphology, whereas secondary granule mRNAs seem to be increased (Dumortier et al., 2003). Thus, increased mRNA levels of granule genes can be considered a leading indicator for obstruction of differentiation. Unfortunately, we cannot explain why the granule mRNA and protein levels are dissociated in neutrophils. One hypothetical explanation is that there are insufficient amounts of translational components for granule synthesis in *Jdp2*$^{-/-}$ neutrophils.

Jdp2 is homologous to ATF3, a negative regulator of TLR signaling, and ATF3 expression is suppressed by Jdp2 in fibroblasts (Weidenfeld-Baranboim et al., 2009). Our genome-wide analysis revealed that the ATF3 promoter region was highly acetylated in *Jdp2*$^{-/-}$ neutrophils. Furthermore, we discovered that Jdp2 directly binds to the ATF3 promoter in neutrophils. Importantly, ATF3 may function as a novel negative regulator of Ly6G. We also revealed that *Jdp2*$^{-/-}$ mice are highly susceptible to infection. The impaired NET formation and ROS production in *Jdp2*$^{-/-}$ neutrophils may be responsible for the increased susceptibility to infection in *Jdp2*$^{-/-}$ mice. Intriguingly, this defect in the in vitro bactericidal function of *Jdp2*$^{-/-}$ neutrophils was mild compared with the highly impaired resistance to *S. aureus* infection. We cannot completely exclude the possibility of defects in other immune cells. Thus, our data suggest the importance of Jdp2 in host defense and also enhance curiosity to clarify the importance of Jdp2 in a wide range of hematopoietic cell functions.

Taken together, we have identified Jdp2 as a critical "osteo-innate-immunological" regulator both in vivo and in vitro. Thus, Jdp2-mediated gene regulation may be a critical target for the development of therapeutics to control abnormal neutrophil- and osteoclast-associated diseases.

EXPERIMENTAL PROCEDURES

Mice, Cells, and Reagents

The generation of *Jdp2*$^{-/-}$ mice is described in the Supplemental Experimental Procedures. Mice were housed in specific-pathogen-free conditions and all animal experiments were carried out with the approval of the animal research committee of the Research Institute for Microbial Diseases (Osaka University). Peritoneal neutrophils were prepared as described (Bertram et al., 2012). B and T cells were isolated from splenocytes with anti-B220 and anti-Thy-1.2 magnetic beads (Miltenyi Biotec), respectively. Splenic dendritic cells (DCs) were isolated with anti-CD11c magnetic beads (Miltenyi Biotec). Primary osteoclasts are prepared as described (Takegahara et al., 2006). Splenic- or bone marrow-derived CD11b^{+}F4/80^{+} macrophages and CD11b^{+}Ly6C^{lo}Ly6G^{+} neutrophils were sorted with a FACSAria (BD Biosciences). Conventional dendritic cells (cDCs) were prepared as described (Kato et al., 2005). *S. aureus* 834 was kindly provided by A. Nakane (Hirosaki University, School of Medicine, Aomori, Japan). This strain was cultured on tryptic soy broth agar plates at 37°C for 24 hr before use. *C. albicans* THK519 was obtained from a patient admitted to Tohoku University Hospital (Sendai, Japan). These cells were cultured on potato dextrose agar (PDA) plates (Eiken) at 30°C for 72 hr before use. The pathogen-associated molecular patterns (PAMPs), Abs, and ELISA kits listed in the Supplemental Experimental Procedures were purchased. Phagocytosis was quantified with a phagocytosis assay kit (500290; Cayman Chemical Company). Superoxide and apoptosis levels were measured with a Diogenes Cellular Luminescence Enhancement System (National Diagnostics) and annexin V-indocarbocyanine (BioVision), respectively.

Analysis of Osteoclastogenesis and Bone Phenotype

For in vitro osteoclast culture, MDMs were generated as described (Maruyama et al., 2006). MDMs were induced to differentiate into osteoclasts in the presence of 25 ng/ml M-CSF and various concentrations of RANKL (R&D Systems). After 3 days, TRAP staining was performed as described (Zhao et al., 2006). For pit assays, MDMs were cultured on bone resorption assay plates (Iwai Chemical Company) with 50 ng/ml RANKL. After 5 days, the plates were immersed in 1 M NH_4OH for 3 hr, and the resorption pits were counted. The in vivo bone phenotype was analyzed as described in the Supplemental Experimental Procedures.

Bone Marrow Transfer

Bone marrow transplantation was performed as described in the Supplemental Experimental Procedures.

qPCR

RNA was extracted from cells with TRIzol (Invitrogen Life Science Technologies), and reverse transcription was performed with ReverTra Ace (Toyobo Co. Ltd.). qPCR was performed in an ABI PRISM 7500 with TaqMan Assay-on-demand primers (Applied Biosystems).

Viral Gene Transfer and RNA Interference

Retroviral or lentiviral gene transfer was performed as described in the Supplemental Experimental Procedures. A siRNA for c-Fos (Stealth RNAi siRNA, MSS247212; Invitrogen) and a control oligo (Stealth RNAi siRNA, negative control Med GC; Invitrogen) were introduced into MDMs with Lipofectamine 2000 (Invitrogen) according to the manufacturer's protocols.

Immunoblotting and Immunoprecipitation

Immunoblotting and immunoprecipitation were performed as described (Kawagoe et al., 2009).

Luciferase Reporter Assay

A C/EBP reporter kit (CCS-001L; QIAGEN) and NFAT reporter kit (CCS-015L; QIAGEN) were used for transient transfection into HEK293 cells with Lipofectamine 2000. Luciferase activities were measured with a Dual-Luciferase Reporter Assay System (Promega), as described (Iwasaki et al., 2011).

Intracellular Calcium Imaging

MDMs were plated on poly-L-lysine-coated glass-bottom dishes and loaded with 5 μM Fura-2/AM for 30 min in loading solution (115 mM NaCl, 5.4 mM KCl, 1 mM $MgCl_2$, 2 mM $CaCl_2$, 20 mM HEPES, 10 mM glucose [pH 7.42]). Fura-2 fluorescent images were analyzed as described (Kuroda et al., 2008).

Immunostaining, FACS, and TEM

Immunostaining of in vitro cultured peritoneal neutrophils was performed essentially as described (Li et al., 2010). Peritoneal neutrophils were stimulated by *S. aureus* or *C. albicans* for 2 hr (MOI = 50) and stained with Hoechst and anti-histone H3 Cit3 Ab (Abcam). Abs for FACS were purchased from BD Biosciences and used for cell staining. Data were acquired in a FACSCalibur (BD Biosciences) and analyzed with FlowJo (Ashland). TEM was performed as described in the Supplemental Experimental Procedures.

Colony Assay

Bone marrow cells were cultured with MethoCult (GFM3434; Stem Cell Technologies) with or without G-CSF (50 ng/ml) supplementation, according to the manufacturer's protocol. After 7 days, the numbers of CFU-G, CFU-M, and CFU-GM were counted.

Microarray, ChIP, and ChIP-seq Analyses

The microarray, ChIP, and ChIP-seq protocols and data analyses are described in the Supplemental Experimental Procedures.

In Vitro and In Vivo Infection

In vitro bacterial killing assays were performed as described in the Supplemental Experimental Procedures. For in vivo infection, *S. aureus* was cultured in tryptic soy broth for 15 hr at 37°C. Cells were collected and suspended in PBS. Mice were infected intravenously with 0.2 ml of solution containing 3×10^7 *S. aureus* cells. *C. albicans* were collected from PDA plates and suspended in PBS. Mice were infected intravenously with 0.2 ml of solution containing 2.5×10^5 *C. albicans* cells. The numbers of viable bacteria in various organs were determined as described (Maruyama et al., 2007).

Statistical Analysis

Student's t test was used to evaluate the significance of differences, with significance set at $p < 0.05$. For survival curves, two groups were compared with a log-rank test.

ACCESSION NUMBERS

The microarray data are available in the Gene Expression Omnibus (GEO) database (http://www.ncbi.nlm.nih.gov/gds) under the accession number GSE42063.

SUPPLEMENTAL INFORMATION

Supplemental Information includes Supplemental Experimental Procedures, six figures, and one table and can be found with this article online at http://dx.doi.org/10.1016/j.immuni.2012.08.022.

ACKNOWLEDGMENTS

We thank S. Tartey and D. Ori for technical advice; E. Kamada and M. Kageyama for secretarial assistance; K. Nojima, Y. Fujiwara, and M. Kumagai for technical assistance; and T. Kawai and Y. Kumagai for fruitful discussions. This work was supported by Special Coordination Funds of the Japanese Ministry of Education, Culture, Sports, Science, and Technology, grants from the Ministry of Health, Labour, and Welfare of Japan, the Japan Society for the Promotion of Science (JSPS) through the Funding Program for World-Leading Innovative R&D on Science and Technology (FIRST Program), and a research fellowship from the JSPS for the Promotion of Science for Young Scientists. K.M. designed and performed most of the experiments. M.F., T.S., T. Kawasaki, T. Kondo, H.K., N.T., and O.T. contributed the immunological experiments. A.V. and D.S. analyzed the ChIP-seq data. K.K.Y. provided the Jdp2 antibody. The manuscript was written by K.M. S.A. supervised the overall research.

Received: May 11, 2012
Accepted: August 16, 2012
Published online: November 29, 2012

REFERENCES

Aronheim, A., Zandi, E., Hennemann, H., Elledge, S.J., and Karin, M. (1997). Isolation of an AP-1 repressor by a novel method for detecting protein-protein interactions. Mol. Cell. Biol. *17*, 3094–3102.

Bertram, A., Zhang, H., von Vietinghoff, S., de Pablo, C., Haller, H., Shushakova, N., and Ley, K. (2012). Protein kinase C-θ is required for murine neutrophil recruitment and adhesion strengthening under flow. J. Immunol. *188*, 4043–4051.

Borregaard, N., and Cowland, J.B. (1997). Granules of the human neutrophilic polymorphonuclear leukocyte. Blood *89*, 3503–3521.

Borregaard, N., Sørensen, O.E., and Theilgaard-Mönch, K. (2007). Neutrophil granules: a library of innate immunity proteins. Trends Immunol. *28*, 340–345.

Brinkmann, V., Reichard, U., Goosmann, C., Fauler, B., Uhlemann, Y., Weiss, D.S., Weinrauch, Y., and Zychlinsky, A. (2004). Neutrophil extracellular traps kill bacteria. Science *303*, 1532–1535.

Colonna, M., Trinchieri, G., and Liu, Y.J. (2004). Plasmacytoid dendritic cells in immunity. Nat. Immunol. *5*, 1219–1226.

Dumortier, A., Kirstetter, P., Kastner, P., and Chan, S. (2003). Ikaros regulates neutrophil differentiation. Blood *101*, 2219–2226.

Forman, H.J., and Thomas, M.J. (1986). Oxidant production and bactericidal activity of phagocytes. Annu. Rev. Physiol. *48*, 669–680.

Hestdal, K., Ruscetti, F.W., Ihle, J.N., Jacobsen, S.E., Dubois, C.M., Kopp, W.C., Longo, D.L., and Keller, J.R. (1991). Characterization and regulation of RB6-8C5 antigen expression on murine bone marrow cells. J. Immunol. *147*, 22–28.

Hock, H., Hamblen, M.J., Rooke, H.M., Traver, D., Bronson, R.T., Cameron, S., and Orkin, S.H. (2003). Intrinsic requirement for zinc finger transcription factor Gfi-1 in neutrophil differentiation. Immunity *18*, 109–120.

Huang, Y.C., Saito, S., and Yokoyama, K.K. (2010). Histone chaperone Jun dimerization protein 2 (JDP2): role in cellular senescence and aging. Kaohsiung J. Med. Sci. *26*, 515–531.

Humphrey, M.B., Daws, M.R., Spusta, S.C., Niemi, E.C., Torchia, J.A., Lanier, L.L., Seaman, W.E., and Nakamura, M.C. (2006). TREM2, a DAP12-associated receptor, regulates osteoclast differentiation and function. J. Bone Miner. Res. *21*, 237–245.

Iwasaki, H., Takeuchi, O., Teraguchi, S., Matsushita, K., Uehata, T., Kuniyoshi, K., Satoh, T., Saitoh, T., Matsushita, M., Standley, D.M., and Akira, S. (2011). The IκB kinase complex regulates the stability of cytokine-encoding mRNA induced by TLR-IL-1R by controlling degradation of regnase-1. Nat. Immunol. *12*, 1167–1175.

Ji, H., Ehrlich, L.I., Seita, J., Murakami, P., Doi, A., Lindau, P., Lee, H., Aryee, M.J., Irizarry, R.A., Kim, K., et al. (2010). Comprehensive methylome map of lineage commitment from haematopoietic progenitors. Nature *467*, 338–342.

Jin, C., Ugai, H., Song, J., Murata, T., Nili, F., Sun, K., Horikoshi, M., and Yokoyama, K.K. (2001). Identification of mouse Jun dimerization protein 2 as a novel repressor of ATF-2. FEBS Lett. *489*, 34–41.

Jin, C., Kato, K., Chimura, T., Yamasaki, T., Nakade, K., Murata, T., Li, H., Pan, J., Zhao, M., Sun, K., et al. (2006). Regulation of histone acetylation and nucleosome assembly by transcription factor JDP2. Nat. Struct. Mol. Biol. *13*, 331–338.

Karsenty, G., and Wagner, E.F. (2002). Reaching a genetic and molecular understanding of skeletal development. Dev. Cell 2, 389–406.

Kato, H., Sato, S., Yoneyama, M., Yamamoto, M., Uematsu, S., Matsui, K., Tsujimura, T., Takeda, K., Fujita, T., Takeuchi, O., and Akira, S. (2005). Cell type-specific involvement of RIG-I in antiviral response. Immunity *23*, 19–28.

Kawagoe, T., Takeuchi, O., Takabatake, Y., Kato, H., Isaka, Y., Tsujimura, T., and Akira, S. (2009). TANK is a negative regulator of Toll-like receptor signaling and is critical for the prevention of autoimmune nephritis. Nat. Immunol. *10*, 965–972.

Kawaida, R., Ohtsuka, T., Okutsu, J., Takahashi, T., Kadono, Y., Oda, H., Hikita, A., Nakamura, K., Tanaka, S., and Furukawa, H. (2003). Jun dimerization protein 2 (JDP2), a member of the AP-1 family of transcription factor, mediates osteoclast differentiation induced by RANKL. J. Exp. Med. *197*, 1029–1035.

Koga, T., Inui, M., Inoue, K., Kim, S., Suematsu, A., Kobayashi, E., Iwata, T., Ohnishi, H., Matozaki, T., Kodama, T., et al. (2004). Costimulatory signals mediated by the ITAM motif cooperate with RANKL for bone homeostasis. Nature *428*, 758–763.

Kuroda, Y., Hisatsune, C., Nakamura, T., Matsuo, K., and Mikoshiba, K. (2008). Osteoblasts induce Ca2+ oscillation-independent NFATc1 activation during osteoclastogenesis. Proc. Natl. Acad. Sci. USA *105*, 8643–8648.

Lagasse, E., and Weissman, I.L. (1996). Flow cytometric identification of murine neutrophils and monocytes. J. Immunol. Methods *197*, 139–150.

Li, P., Li, M., Lindberg, M.R., Kennett, M.J., Xiong, N., and Wang, Y. (2010). PAD4 is essential for antibacterial innate immunity mediated by neutrophil extracellular traps. J. Exp. Med. *207*, 1853–1862.

Lieschke, G.J., Grail, D., Hodgson, G., Metcalf, D., Stanley, E., Cheers, C., Fowler, K.J., Basu, S., Zhan, Y.F., and Dunn, A.R. (1994). Mice lacking granulocyte colony-stimulating factor have chronic neutropenia, granulocyte and macrophage progenitor cell deficiency, and impaired neutrophil mobilization. Blood *84*, 1737–1746.

Martinelli, S., Urosevic, M., Daryadel, A., Oberholzer, P.A., Baumann, C., Fey, M.F., Dummer, R., Simon, H.U., and Yousefi, S. (2004). Induction of genes mediating interferon-dependent extracellular trap formation during neutrophil differentiation. J. Biol. Chem. *279*, 44123–44132.

Maruyama, K., Takada, Y., Ray, N., Kishimoto, Y., Penninger, J.M., Yasuda, H., and Matsuo, K. (2006). Receptor activator of NF-kappa B ligand and osteoprotegerin regulate proinflammatory cytokine production in mice. J. Immunol. *177*, 3799–3805.

Maruyama, K., Sano, G., Ray, N., Takada, Y., and Matsuo, K. (2007). c-Fos-deficient mice are susceptible to *Salmonella enterica serovar Typhimurium* infection. Infect. Immun. *75*, 1520–1523.

Nishikawa, K., Nakashima, T., Hayashi, M., Fukunaga, T., Kato, S., Kodama, T., Takahashi, S., Calame, K., and Takayanagi, H. (2010). Blimp1-mediated repression of negative regulators is required for osteoclast differentiation. Proc. Natl. Acad. Sci. USA *107*, 3117–3122.

Nishinaka, Y., Arai, T., Adachi, S., Takaori-Kondo, A., and Yamashita, K. (2011). Singlet oxygen is essential for neutrophil extracellular trap formation. Biochem. Biophys. Res. Commun. *413*, 75–79.

Takayanagi, H. (2007). Osteoimmunology: shared mechanisms and crosstalk between the immune and bone systems. Nat. Rev. Immunol. *7*, 292–304.

Takegahara, N., Takamatsu, H., Toyofuku, T., Tsujimura, T., Okuno, T., Yukawa, K., Mizui, M., Yamamoto, M., Prasad, D.V., Suzuki, K., et al. (2006). Plexin-A1 and its interaction with DAP12 in immune responses and bone homeostasis. Nat. Cell Biol. *8*, 615–622.

Weidenfeld-Baranboim, K., Hasin, T., Darlyuk, I., Heinrich, R., Elhanani, O., Pan, J., Yokoyama, K.K., and Aronheim, A. (2009). The ubiquitously expressed bZIP inhibitor, JDP2, suppresses the transcription of its homologue immediate early gene counterpart, ATF3. Nucleic Acids Res. *37*, 2194–2203.

Yamanaka, R., Barlow, C., Lekstrom-Himes, J., Castilla, L.H., Liu, P.P., Eckhaus, M., Decker, T., Wynshaw-Boris, A., and Xanthopoulos, K.G. (1997). Impaired granulopoiesis, myelodysplasia, and early lethality in CCAAT/enhancer binding protein epsilon-deficient mice. Proc. Natl. Acad. Sci. USA *94*, 13187–13192.

Zhang, P., Iwama, A., Datta, M.W., Darlington, G.J., Link, D.C., and Tenen, D.G. (1998). Upregulation of interleukin 6 and granulocyte colony-stimulating factor receptors by transcription factor CCAAT enhancer binding protein alpha (C/EBP alpha) is critical for granulopoiesis. J. Exp. Med. *188*, 1173–1184.

Zhao, C., Irie, N., Takada, Y., Shimoda, K., Miyamoto, T., Nishiwaki, T., Suda, T., and Matsuo, K. (2006). Bidirectional ephrinB2-EphB4 signaling controls bone homeostasis. Cell Metab. *4*, 111–121.

Oncogene (2013) 32, 414–421

www.nature.com/onc

ORIGINAL ARTICLE

microRNA-125b inhibits tube formation of blood vessels through translational suppression of VE-cadherin

F Muramatsu[1,3], H Kidoya[1,3], H Naito[1], S Sakimoto[1] and N Takakura[1,2]

Angiogenesis is controlled positively or negatively by extrinsic and intrinsic molecular cues in endothelial cells (ECs); in the tumor microenvironment, the action of positive regulators exceeds that of negative regulators. Thus, overinduction of negative regulators may inhibit tumor angiogenesis. MicroRNAs (miRNAs or miRs) are endogenous short noncoding RNAs regulating gene expression either through translational inhibition or destabilization of target mRNA. Here, we show that miR-125b expression is transiently induced in ECs on stimulation with vascular endothelial growth factor or by ischemia. miR-125b inhibits translation of *vascular endothelial (VE)-cadherin* mRNA and *in vitro* tube formation by ECs. Injection of miR-125b into the tumor inhibited VE-cadherin expression by ECs and induced nonfunctional blood vessel formation, resulting in inhibition of tumor growth. It has been suggested that pro-angiogenic signals in ECs also upregulate anti-angiogenic molecules simultaneously via negative feedback. Because miR-125b induction in ECs is transient after pro-angiogenic stimulation, prolonged overexpression of miR-125b could result in blood vessel regression. Thus, miR-125b may be useful in cancer therapy by causing the collapse of the lumen of ECs.

Oncogene (2013) **32,** 414–421; doi:10.1038/onc.2012.68; published online 5 March 2012

Keywords: microRNA; mir125b; angiogenesis; VE-cadherin

INTRODUCTION

In the initial step of angiogenesis, mural cells overlying endothelial cells (ECs) dissociate from them, and the ECs start to migrate and proliferate.[1] Therefore, at the onset of angiogenesis, regulators associated with blood vessel maintenance need to be transiently suppressed. ECs proliferate on stimulation with growth factors, especially vascular endothelial growth factor (VEGF), while simultaneously such factors induce upregulation of molecular cues that disrupt blood vessel stability.[2] However, expression of such molecules does not persist for the whole period of growth and maturation of blood vessels during angiogenesis.

For stabilization of blood vessels under normoxia, mural cells such as pericytes or vascular smooth muscle cells must adhere to ECs. This process of mural cell recruitment is triggered mainly by platelet-derived growth factor-B produced by ECs.[3] Subsequently, angiopoietin-1 (Ang1) produced by mural cells directly stimulates Tie2, a tyrosine kinase receptor expressed on ECs, resulting in cell-to-cell adhesion between mural cells and ECs.[4–7] Under hypoxia, for induction of angiogenic switching in pre-existing blood vessels, Ang2, an antagonist of Ang1 produced by ECs, inhibits phosphorylation of Tie2, followed by mural cell dissociation from ECs.[8] This process is thought to be essential for initiation of sprouting angiogenesis.

In addition to dissociation of mural cells from ECs, it is believed that transient disruption of the integrity of cell-to-cell binding is required to induce angiogenesis via transcellular extravasation into ischemic or inflammatory foci of proangiogenic hematopoietic cells as an accessory cell component.[9] EC-to-EC contact is regulated by different adhesion molecules, among which vascular endothelial (VE)-cadherin in particular plays essential roles in the formation of adherens junctions and in permeability control.[10] It was shown to be essential for the formation of stable blood vessels[11–13] and is also important for EC tube formation, inducing tube-like structures even when expressed in melanoma tumor cells.[14] Phosphorylation or endocytosis of VE-cadherin induced by activation of the VEGF receptor has been suggested to attenuate barrier function of ECs for leukocyte transmigration through the EC monolayer.[9] However, whether the transcription or translation of VE-cadherin is affected by VEGF has not been well established.

MicroRNAs (miRNAs or miRs) are endogenous short noncoding RNAs regulating gene expression either through translational inhibition or destabilization of target mRNA.[15] Crucial roles of miRNAs have been reported for many aspects of development, homeostasis and disease including tumor development.[16] Several lines of evidence suggest the involvement of miRNA in blood vessel formation.[17] Therefore, in the present study, we searched for miRNAs that are transiently endogenously upregulated in ECs on angiogenic switching and could inhibit angiogenesis if continuously overexpressed.

RESULTS

MiR-125b is upregulated in ECs under hypoxia or on stimulation with VEGF and inhibits their *in vitro* tube formation

We first analyzed the expression of miRs in ECs from hindlimb muscle subjected to hypoxia by the occlusion of the femoral artery. At 1 day after induction of ischemia, primary ECs ($CD31^+CD45^-$) from hindlimb muscles of mice were isolated by fluorescence-activated cell sorting. ECs from hindlimb muscle in the steady state acted as controls to compare the expression of miRs. Based on earlier reports of which miRs are expressed in ECs under different conditions,[17] we evaluated the expression of 20 miRs using

[1]Department of Signal Transduction, Research Institute for Microbial Diseases, Osaka University, Osaka, Japan and [2]JST, CREST, Tokyo, Japan. [3]These two authors contributed equally to this work. Correspondence: Professor N Takakura, Department of Signal Transduction, Research Institute for Microbial Diseases, Osaka University, 3-1 Yamada-oka, Suita, Osaka 565-0871, Japan. E-mail: ntakaku@biken.osaka-u.ac.jp
Received 7 March 2011; revised 27 January 2012; accepted 29 January 2012; published online 5 March 2012

quantitative reverse-transcription real-time PCR (qRT-PCR) analysis. Of these, we found that miRs 15b, 20b, 29a, 99a, 100, 103, 106b, 125b, 191 and 222 were increased by hypoxia (Figure 1a). We hypothesized that tumor cells may negatively regulate miRs that induce regression of blood vessels. Of the miRs overexpressed in ECs under tissue hypoxia, miRs 29a, 103 and 125b have been reported to be decreased in co-culture with tumor cells.[18] Here, we investigated the function of these miRs, as well as of miR-181a, which decreased in ECs either on hindlimb ischemia or co-culture with tumor cells, using *in vitro* tube formation of human umbilical vein ECs (HUVECs) as a readout. The results suggest that only miR-125b inhibits tube formation (Figure 1b). Therefore, we focused on miR-125b to study associations with angiogenesis.

Because miR-125b is upregulated in primary ECs under tissue hypoxia, we established the kinetics of its expression compared with miR-92a, which has been reported to be upregulated in ECs upon tissue hypoxia,[19] and snoRNA202, which is widely used as a nonregulated gene in various tissues. As shown in Figure 1c, miR-125b expression was transiently increased in ECs at 1 day after induction of ischemia and returned to basal level from day 2. miR-92a was also increased 1 day after induction of ischemia and gradually decreased thereafter.

Next, we assessed the expression of miR-125b in cultured HUVECs and tested whether this miR is upregulated upon angiogenic stimuli or hypoxia. First, we quantified the expression of miR-125b compared with miR-126, which is abundantly expressed specifically in ECs,[20] as well as with other miRs (Supplementary Figure S1). We found that miR125b is not highly expressed in HUVECs under the usual culture conditions. However, as with tissue hypoxia *in vivo*, we found that pro-angiogenic VEGF stimulation, as well as hypoxia (1.5% O_2), transiently induced miR-125b expression in cultured HUVECs (Figure 2a). VEGF is upregulated in ECs under tissue hypoxia. Therefore, hypoxia-mediated VEGF production in HUVECs may itself directly induce miR125b. However, hypoxia-induced miR125b is expressed earlier than VEGF in HUVECs, suggesting that other molecular cues associated with hypoxia induce miR125b. Moreover, basic fibroblast growth factor, a known pro-angiogenic factor, also induced miR-125b expression. Taken together, these data suggest the involvement of several growth factors for induction of miR-125b under conditions of tissue hypoxia similar to those that induce angiogenesis.

As recently reported, VEGF enhances the expression of p53,[21] and because several miRs are induced by p53 with the Drosha complex,[22,23] we tested whether miR125b expression is regulated by p53 in ECs. Small interfering RNA-mediated p53 knockdown inhibited VEGF-mediated induction of miR125b as well as constitutive expression of this miR (Figure 2b and Supplementary Figure S2).

a

ischemia/sham vascular EC miRNA expression change			
miRNA	**fold change↑**	**miRNA**	**fold change↓**
miR-15b	2.7	miR-16	0.07
miR-20b	91.9	miR-24	0.50
miR-29a	100.9	miR-31	0.09
miR-99a	12.6	miR-106a	0.14
miR-100	6.8	miR-125a	0.12
miR-103	30.3	miR-126-3p	0.40
miR-106b	9.02	miR-130a	0.11
miR-125b	2.03	miR-181a	0.20
miR-191	2.2	miR-221	0.36
miR-222	14.3	miR-320	0.14

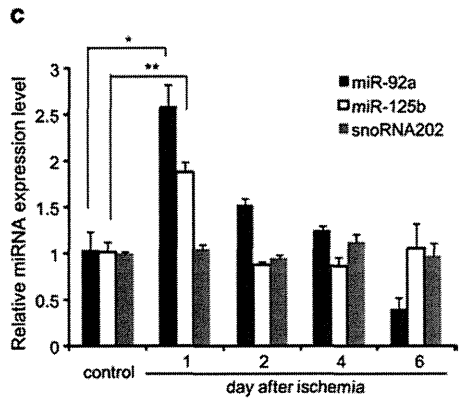

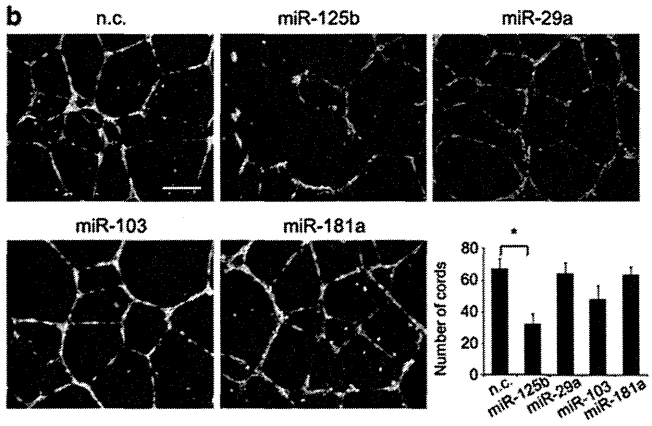

Figure 1. Screening of miRNAs upregulated on hypoxia and inhibiting EC tube formation. (**a**) List of significantly increased (fold change >2.0) or decreased (fold change o 0.5) miRs in ECs affected by hindlimb ischemia. Mice were killed 24 h after induction of ischemia and $CD45^{-}CD31^{+}$ ECs from hindlimb muscle of three mice were sorted and pooled. The data are representative of one of three sets of experiments. Expression of each miR was normalized to RNU6, which is stably expressed under both tissue hypoxia and normoxia. (**b**) Screening for miRs inhibiting HUVEC tube formation. miRs including control miR (n.c.) as indicated were transfected into HUVECs. After 5 h, the cells were cultured for 20 h in Humedia EG2. They were then harvested, cultured for 10 h in 24-well plates coated with Matrigel and analyzed for tubule branching. For quantitative evaluation, we calculated the number of branches in six random fields. Bar indicates 200 μm. *Po 0.05 (n=3). (**c**) Time course of miR-125b expression analyzed by qRT-PCR in ECs from the hindlimb ischemia model. miR125b expression was compared with miR92a and snoRNA202 expression. snoRNA202 was used as a nonregulated gene in various tissues. ECs from three mice per experimental condition were pooled as in (**a**). Data show relative miR-125b or miR-92a expression, taking each miR in the steady state as unity. *Po 0.01, **Po 0.05 (n=3).

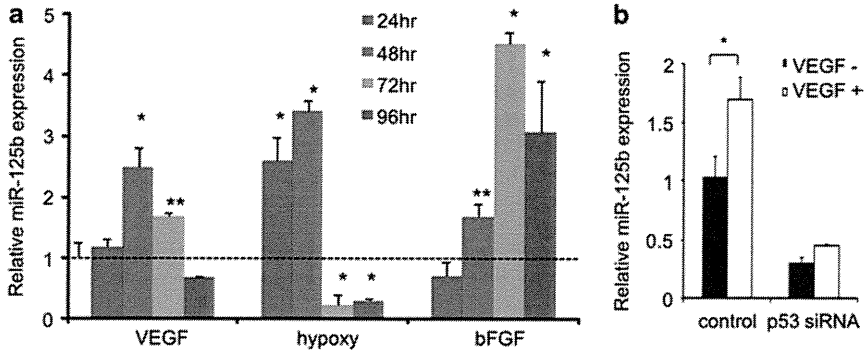

Figure 2. Induction of miR-125b expression in ECs by VEGF. (**a**) Induction of miR-125b expression in HUVECs. 2×10^5 HUVECs in six-well culture plates were serum starved for 6 h by culturing in Humedia EG2 without growth factors, and cultured in the presence or absence of VEGF (10 ng/ml) or basic fibroblast growth factor (bFGF; 5 ng/ml) or under hypoxic conditions (1.5% O_2) for the indicated times. miR-125b expression level by qRT-PCR was normalized to RNU6 using the comparative threshold cycle method. Level of miR-125b expression before stimulation with several factors was set as one. *P< 0.01, **P< 0.05 (n = 3). (**b**) miR-125b expression in HUVECs after p53 knockdown with RNA interference (RNAi). HUVECs were cultured in the presence or absence of VEGF for 24 h. *P< 0.05 (n = 3).

MiR-125b inhibits translation of VE-cadherin mRNA

It has been reported that miR-125b suppresses the expression of Her2 (human epidermal growth factor receptor-related 2) and Bak1 (BCL2-antagonist/killer 1),[24,25] but there are no reports on angiogenesis-related gene expression regulation by miR-125b. We employed several miR target prediction algorithms to identify putative miR-125b targets. We identified *VE-cadherin* as a target with a potential conserved binding site within its 3′ untranslated region (3′UTR) screened by TargetScan (Whitehead Institute for Biomedical Research, Cambridge, MA, USA); this sequence is evolutionarily conserved (Figure 3a). VE-cadherin is involved in tube formation by ECs by providing the adhesive component of endothelial adherens junctions.[2,9,10] Based on our results on tube formation in matrigel (Figure 1b), we hypothesized that miR-125b might downregulate synthesis of VE-cadherin by directly binding to sites within the 3′UTR of its message. To assess this possibility, we constructed luciferase reporter vectors encoding the complete wild-type 3′UTR of VE-cadherin mRNA as well as parallel control vectors containing mismatches in the predicted miR-125b binding site, or luciferase vectors containing no VE-cadherin UTR. As shown in Figure 3b, co-transfection of miR-125b with the luciferase reporter gene linked to the wild-type 3′UTR of human or mouse VE-cadherin resulted in a significant decrease in luciferase activity. In contrast, co-transfection of miR-125b with constructs containing mutated 3′UTR sequences did not result in decreased luciferase activity.

To confirm miR-125b-mediated modulation of endogenous VE-cadherin in ECs, HUVECs were transfected with miR-125b or control miR and expression of VE-cadherin on HUVECs assessed by western blotting and flow cytometry. An ~60% decrease of VE-cadherin expression resulted from the induction of miR-125b, using precursor molecules (pre-miR) (Figures 3c and d). We confirmed a reduction of cell surface VE-cadherin expression by flow cytometry (Figure 3e). We could not detect any alteration of VE-cadherin mRNA expression caused by miR-125b (Figure 3f). Indeed, inhibition of tube formation by miR-125b was abrogated by the overexpression of VE-cadherin (Figures 4a and b and Supplementary Figure S3); miR-125b inhibition did not enhance VE-cadherin expression (data not shown).

MiR-125b inhibits tumor growth mediated by severe hypoxia through disruption of EC tube formation

The results described above suggested that introduction of miR-125b into the tumor would inhibit angiogenesis and tumor growth. Before assessing the *in vivo* anti-angiogenic effect of injecting miR-125b into tumors, we tested its effects on tumor cells *in vitro*. Although it had been previously reported that miR-125b attenuated ErbB2 (erythroblastic leukemia viral oncogene homolog 2) expression and decreased proliferation of breast cancer cells *in vitro*,[24] our experiments failed to demonstrate any inhibitory effects of miR-125b on these parameters in Lewis lung carcinoma (LLC) or colon-26 cancer cells (Supplementary Figure S4).

We inoculated mice subcutaneously with tumor cells and started to inject miR-125b directly into the tumor using non-viral vectors composed of the cationic polymer polyethylenimine[26] when the tumor volume had reached 100 mm^3 (LLC: Figure 5) or 80 mm^3 (colon-26: supplementary Figure S5). Several weeks after injection of miR-125b, clear differences in the size of LLC and colon-26 tumors could be discerned (Figures 5a and b and Supplementary Figure S5a and b), but there were no differences between control and anti-miR-125-treated groups. In the group treated with anti-miR-125b, tumor growth might have been expected to increase compared with control because of the possibility of VE-cadherin expression enhancement. However, anti-miR-125b treatment did not markedly enhance VE-cadherin expression in the tumor environment. Moreover, we confirmed that enhancement of VE-cadherin expression was also not induced in HUVECs by anti-miR-125b transfection. Our study suggests that the level of miR-125b expression in tumor ECs is slightly upregulated (o 2.0-fold) but is not markedly higher than in ECs in normal skin, and that its localization therein is random, with no specific expression profile (data not shown). Therefore, anti-miR-125b may not enhance VE-cadherin expression in the tumor.

Real-time RT-PCR analysis confirmed significantly higher levels of miR-125b expression in tumors injected with miR-125b (Figure 5c and Supplementary Figure S5c). Essentially all $CD31^+$ ECs in control tumors expressed VE-cadherin, but in the miR-125b-transfected tumors, VE-cadherin expression by the majority of $CD31^+$ ECs was greatly reduced around the area of miR-125b injection (Supplementary Figure S6). Analysis of single-cell suspensions from each tumor confirmed the attenuation of endothelial VE-cadherin expression in miR-125b-injected tumors compared with controls (Figure 5d).

The miR-125b treatment significantly reduced the number of blood vessels in the tumor, but the difference was not marked (Figures 6a and b). On the other hand, morphological studies revealed indented irregular shaped blood vessels in miR-125b-injected tumors, not seen in controls. Moreover, we commonly found blood vessels stained with CD31 in miR-125b-treated tumors that were not stained by *in vivo* lectin perfusion, indicating lack of blood flow through them (Figure 6a). Assessing the state of

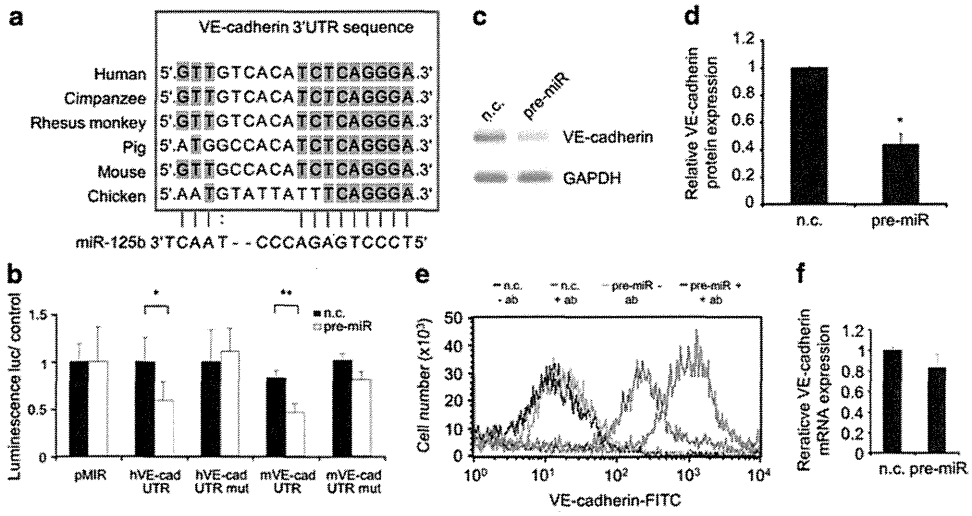

Figure 3. VE-cadherin is a direct target of miR-125b. (**a**) Alignment of potential miR-125b binding sites in the 3′UTR of the VE-cadherin mRNA of different species. (**b**) pMIR-REPORT vectors containing the 3′UTR of genes for wild-type human (h) or mouse (m) VE-cadherin (h or mVE-cad UTR) or mutated miR-125b binding site (h or mVE-cad UTR mut) and miR-125b (pre-miR) or control miR (n.c.) were co-transfected into HEK293 cells. The pMIR-REPORT vector containing no 3′UTR (pMIR) was used as a control set to unity. *P$_o$ 0.05, **P$_o$ 0.01 ($n=3$). (**c**) Western blot analysis of VE-cadherin expression in HUVECs transfected with control miR (n.c.) or miR-125b (pre-miR). Cell lysates were from HUVECs 48 h after transfection. GAPDH was used as an internal control. (**d**) Quantitative evaluation of VE-cadherin expression analyzed as described in (**c**). *P$_o$ 0.01 ($n=5$). (**e**) Cell surface expression of VE-cadherin in HUVECs treated as described in (**c**). Cells were stained with propidium iodide (PI) and fluorescein isothiocyanate (FITC)-conjugated anti-VE-cadherin antibody and analyzed by flow cytometry. PI-nonstained living cells were analyzed. −ab, cells stained by isotype-matched control IgG; + ab, cells stained with FITC-conjugated anti-VE-cadherin antibody. (**f**) qRT-PCR analysis of VE-cadherin expression in HUVECs transfected with control miR (n.c.) or miR-125b (pre-miR). mRNA was isolated 24 h after transfection of miR. The relative abundance of transcripts was normalized using the expression level of GAPDH mRNA. Error bar; there are no statistically significant differences ($n=3$).

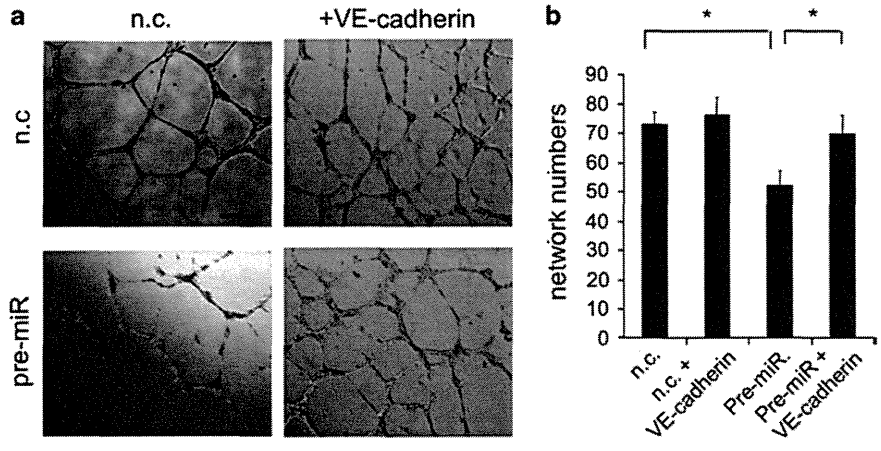

Figure 4. Rescue experiments. VE-cadherin overexpression in ECs transfected with miR-125b. (**a**) HUVECs transfected with control miR (n.c.) or miR-125b (pre-miR) with or without VE-cadherin expression vector assessed for tube formation. HUVECs were cultured for 20 h in Humedia EG2. Cells were then harvested and cultured for 10 h in 24-well plates coated with Matrigel. VE-cadherin almost completely rescued the miR-125b-induced decrease of tube formation. Bar indicates 200 μm. (**b**) For quantitative evaluation, we calculated the number of branches in six random fields. *P$_o$ 0.05.

hypoxia using hypoxyprobe showed that miR-125b-treated tumors were more hypoxic than controls (Figures 7a and b). Therefore, we concluded that miR-125b-suppressed VE-cadherin expression in ECs resulted in inhibition of tube formation, and because severe hypoxia is thus induced in the tumor environment, miR-125b inhibits tumor growth.

DISCUSSION

Here we report that miR-125b is upregulated in hypoxic ECs or on stimulation with VEGF or basic fibroblast growth factor. p53 is a regulator of miR-125b induction, but other mechanisms regulating its expression are also likely to exist. miR-125b binds directly to the 3′UTR of VE-cadherin mRNA and inhibits its translation. In contrast to upregulation of miR-125b expression, miR-125a was downregulated in ECs upon hypoxia. The seed sequences of miR-125a and miR-125b are identical, and downregulation of miR-125a may affect VE-cadherin expression; however, we focused on miR-125b, because we were seeking miRs that were upregulated and affected angiogenesis upon hypoxia.

When miR-125b is induced in ECs, their *in vitro* tube formation is suppressed by a mechanism involving inhibition of VE-cadherin

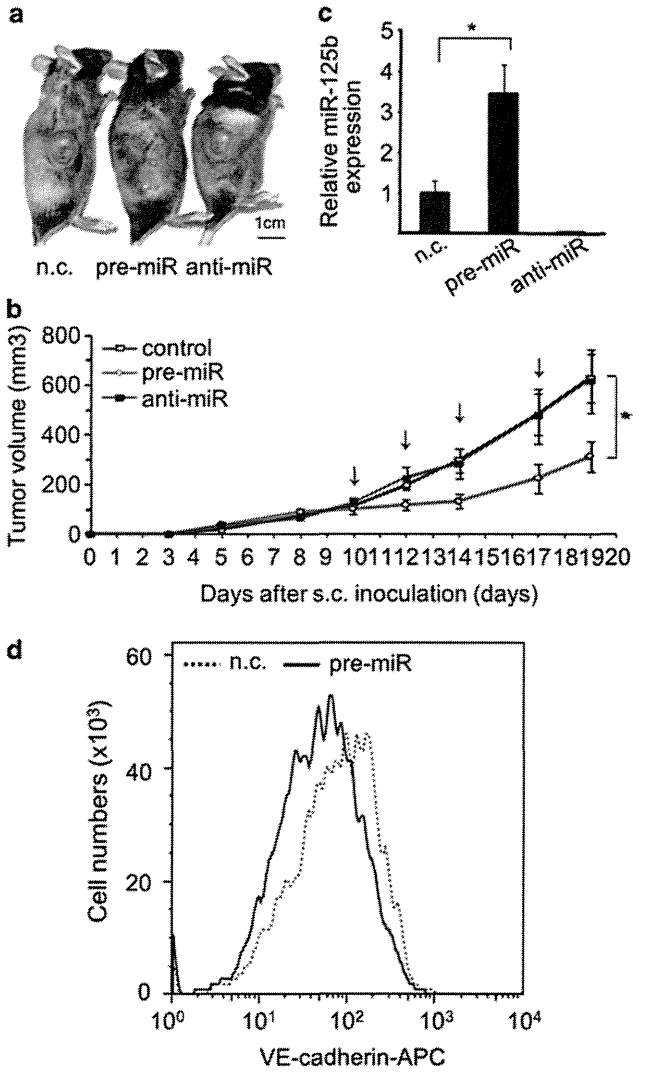

Figure 5. Suppression of tumor outgrowth by miR-125b. (**a**) Gross appearance of tumor-bearing mice 20 days after tumor cell inoculation. LLC cells (3×10^6) were inoculated subcutaneously into C57BL/6 mice. Anti-miR, anti-miR-125b; n.c., negative control; pre-miR, miR-125b. (**b**) Tumor growth suppressed by miR-125b but not by anti-miR-125b. Arrows indicate the day of miR injection. Tumor growth was monitored by calculating tumor volume on days 10, 12, 14, 17 and 19 after injection of miR-125 (pre-miR), anti-miR-125b (anti-miR) or negative control (control). *P$_0$ 0.05 (n = 3). (**c**) Detection of miR-125b expression in the tumor. At 2 days after injection of miR-125b, total RNA from tumor was isolated. A 3.5-fold increased level of miR-125b in the miR-125 (pre-miR)-injected group compared with the control miR (n.c.) group is seen. Anti-miR-125b suppressed the endogenous expression of miR-125b. Values normalized to RNU6 expression in each tumor were compared with the values obtained from the n.c. set at unity. *P$_0$ 0.01 (n = 3). (**d**) Suppression of VE-cadherin expression on ECs in the tumor. Single-cell suspensions from tumors injected with control miR (n.c.) or miR-125b (pre-miR) as described in (**a**) were stained with anti-VE-cadherin and anti-CD31 monoclonal antibodies (mAbs) and analyzed by flow cytometry. VE-cadherin expression on CD31-positive cells was analyzed. Mean intensity of VE-cadherin expression in these two groups was significantly different (P$_0$ 0.05, n = 5). The data shown are representative.

expression. This is confirmed by the finding that preceding overexpression of VE-cadherin in ECs prevents this suppression of tube formation by miR-125b. By blocking VE-cadherin expression in tumor ECs, miR-125b inhibited tumor outgrowth by disrupting EC tube formation. Although our studies have focused on ECs, we cannot completely exclude the possibility that miR-125b also affects other cell types in the tumor environment. However, as far as we could determine, miR-125b had no effect on tumor cell proliferation itself.

Induction of miR-125b expression in ECs of ischemic hindlimb muscle is transient, suggesting that miR-125b may have a role at the onset of angiogenesis in loosening EC contacts to allow extravasation of proangiogenic hematopoietic cells or bone marrow vascular progenitors into ischemic foci. We previously reported that many hematopoietic cells infiltrate into tumor sites from the edge of the tumor and that inhibition of migration of hematopoietic cells into the tumor inhibited tumor angiogenesis.[27] It is well known that hematopoietic cells can exert proangiogenic activity as an accessory cell component and that infiltration of these cells into the tumor environment occurs before ECs form blood vessels in the tumor.[27,28] Vascular endothelial cell-specific phosphotyrosine phosphatase (VE-PTP) is a phosphatase suppressing phosphorylation of VE-cadherin. Lack of VE-PTP leads to constitutive activation of VE-cadherin, resulting in suppression of normal angiogenesis.[29] Suppression of VE-cadherin function enhances the extravasation of hematopoietic cells.[30] Interestingly, pretreatment with anti-miR-125b in a tumor xenograft model led to retardation of tumor growth (Supplementary Figure S7). Moreover, preinduction of anti-miR-125b in HUVECs led to suppression of endothelial sprouting in a model using endothelial spheroids (Supplementary Figure S8). These findings suggest that transient downregulation of VE-cadherin expression is required for initiation of angiogenesis and that miR-125b may be involved in this process. However, further analysis is required to clarify the physiological function of miR-125b.

At the initiation of angiogenesis, it is widely accepted that Ang2, an antagonist of Ang1 that maintains stability of blood vessels by cell-to-cell adhesion between mural cells and ECs through the Tie2 receptor, is released from ECs to destabilize the vessels.[7,8] Hence, transient Ang2 expression is required for initiating angiogenesis, but its prolonged expression results in blood vessel regression under physiological or pathological conditions.[31] Thus far, no molecules other than Ang2 participating in transient destabilization of preexisting blood vessels have been identified. As tissue hypoxia or VEGF induces miR-125b expression in ECs, this miR may be involved in the initiation of angiogenesis by suppression of VE-cadherin expression. Although it is possible that the anti-angiogenic factor miR-125b is merely upregulated upon stimulation by pro-angiogenic factors as a negative feedback mechanism, but is not required for initiation of sprouting angiogenesis, our data suggest that excessively prolonged miR-125b expression prevents EC tube formation, leading to inhibition of tumor growth as observed in the Tie2/Ang2 system.

Our study suggests that ECs in the tumor environment express a little more miR-125b than other ECs. Nonetheless, the level of expression of miR125b was not particularly high, as described above. This is consistent with our initial hypothesis that tumor cells suppress expression of molecules in the tumor environment, which would mitigate against tumor growth. Indeed, when HUVECs were co-cultured with tumor cells, miR-125b expression was downregulated. Although this finding has already been reported by another group,[18] we found that VEGF co-stimulation in co-cultures of HUVECs and tumor cells resulted in slightly upregulated miR-125b expression in the former. However, the level of expression of this miR did not exceed the original level in HUVECs (Supplementary Figure S9). Therefore, tumor cell-derived factors must oppose VEGF effects for upregulation of miR-125b in ECs.

Molecular analysis of miRs has progressed rapidly and application of miRs in cancer therapy is being considered. One line of evidence showed involvement of miR-92a in vascular integrity by means of regulating the integrin subunit α-5, known to play an important role in angiogenesis.[19] It is suggested that

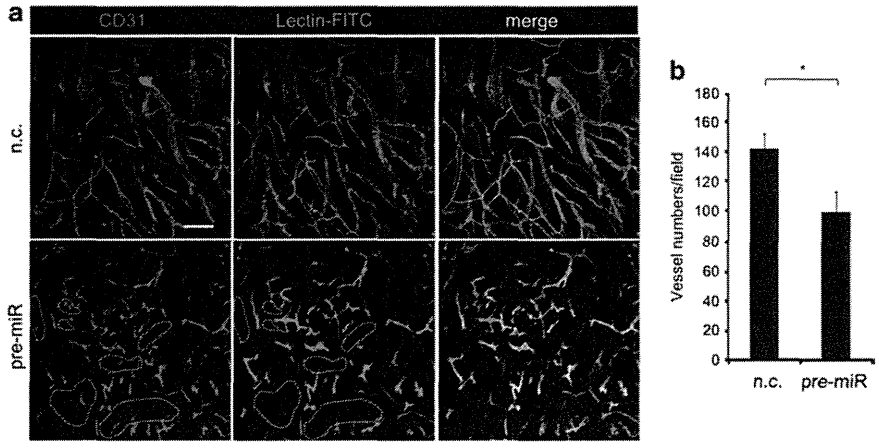

Figure 6. Disorganized structure of blood vessels induced by miR-125b. (**a**) ECs visualized with anti-CD31 antibody (red) and lectin staining (green) in the tumor. Treatment with miR-125b (pre-miR) induced disorganized vessel structure and blood vessels without blood flow (dashed area) suggesting nonfunctional blood vessels. n.c., negative control. Bar indicates 100 μm. (**b**) Quantitative evaluation of the number of lectin$^+$ blood vessels in n.c. or miR-125b-injected tumor, showing representative data for the number of blood vessels calculated in six random fields from one tumor of seven independent experiments. *P< 0.01.

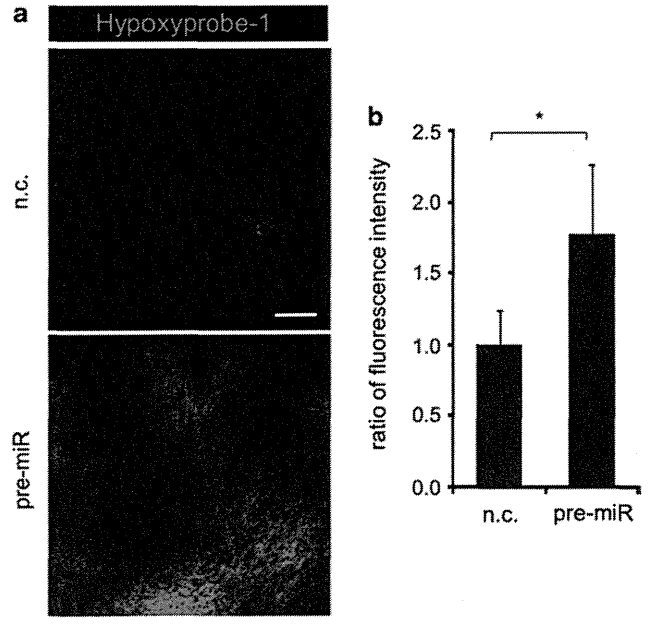

Figure 7. Hypoxia was induced by miR-125b injection. (**a**) Sections from tumors injected with control miR (n.c.) or miR-125b (pre-miR) were stained with anti-hypoxyprobe-1 (green). Hypoxyprobe-1 was injected into the peritoneal cavity before dissection. Bar indicates 50 μm. (**b**) Quantitative evaluation of the degree of hypoxia. The intensity of green fluorescence was measured using NIH image software (Bethesda, MD, USA) in 20 random fields. *P< 0.01.

overexpression of miR-92a inhibits angiogenesis by attenuating α-5 integrin expression in ischemic tissue. We found that miR92a is also transiently upregulated in ECs upon tissue hypoxia. Taken together with the results of the miR-125b study, it is suggested that miRNAs upregulated in ECs at the onset of angiogenesis may have an anti-angiogenic function; thus, it may be useful to identify anti-angiogenic miRs by this method. Using delivery of miRs directly into ECs in the tumor environment, miR-125b should be a good candidate for inhibition of tumor angiogenesis.

MATERIALS AND METHODS

Animals and cells

C57BL/6 mice were purchased from Japan SLC (Shizuoka, Japan). Animals were housed in environmentally controlled rooms of the animal experimentation facility at Osaka University. All experiments were carried out following the guidelines of Osaka University Committee for animal and recombinant DNA experiments. HUVECs (Kurabo, Osaka, Japan) were cultured in Humedia EG2. HUVECs were grown to confluence, serum starved and stimulated with VEGF (10 ng/ml; PeproTech, Rocky Hill, NJ, USA). Analyses such as of tube formation were performed as described.[32] LLC cells were maintained in Dulbecco's modified Eagle's medium (Sigma, St Louis, MO, USA) with 10% fetal bovine serum (Sigma) and penicillin/streptomycin (GIBCO, Rockville, MD, USA). A murine hindlimb ischemia model was established by the occlusion of the femoral artery as previously reported.[33] Sorting of primary ECs (CD31$^+$ CD45$^-$) from hindlimb muscle or tumor tissues was performed using a JSAN flow cytometer (Bay Bioscience, Kobe, Japan) as reported previously.[32] Tumor cell xenograft model was also as previously reported.[34] Preparation of single-cell suspensions from tumors and flow cytometric analysis were performed as previously described.[35]

Quantitative reverse-transcription real-time PCR

For miRs assessments, total RNA was extracted using PureLink miRNA Isolation Kits (Invitrogen, Carlsbad, CA, USA) and subjected to reverse transcription with the NCode miRNA First-Strand cDNA Synthesis and qRT-PCR Kits (Invitrogen) according to the manufacturer's instructions. qRT-PCR was performed with the Mx3000P QPCR System (Agilent Technologies Inc., Santa Clara, CA, USA) using Platinum SYBR Green qPCR SuperMix-UDG (Invitrogen). Results were normalized to RNU6 using the comparative threshold cycle method. Specific primers used in this experiment are described in Supplementary Table S1.

For detection of mRNA, total RNA was extracted using RNeasy mini kits (QIAGEN, Valencia, CA, USA) and reverse transcribed using the PrimeScript RT reagent Kit (Takara, Otsu, Japan) according to the manufacturer's instructions. qRT-PCR was performed as described above. Results were normalized to GAPDH (glyceraldehyde-3-phosphate dehydrogenase) with the comparative threshold cycle method. Specific primers used in this experiment were as follows: human VE-cadherin: 5′-ATCGGTTGTT CAATGCGTCC-3′ (sense) and 5′-CCTTCAGGATTTGGTACATGACA-3′ (anti-sense); human GAPDH: 5′-GAAGGTGAAGGTCGGAGTC-3′ (sense) and 5′-GAAGATGGTGATGGGATTTC-3′(anti-sense), and human p53: 5′-CTTCG AGATGTTCCGAGAGC-3′ (sense) and 5′-TTATGGCGGGAGGTAGACTG-3′ (anti-sense).

Transfection of plasmid, RNA interference and miRNA

For overexpression of miRs, 33 nM pre-miRs 125-b, 29a, 103 and 181a or pre-miR-control (Applied Biosystems, Foster City, CA, USA) were transfected into HUVECs using Lipofectamine 2000 (Invitrogen). After 5 h, the cells were cultured in Humedia EG2 until further analysis. For knockdown of p53, small interfering RNA (TP53 stealth select RNA interference; Invitrogen) or control small interfering RNA (Invitrogen) was introduced into HUVECs as described above. For the rescue experiment of VE-cadherin, the human VE-cadherin expression vector (a kind gift of Dr Fukuhara, NCVC, Osaka, Japan) was introduced into HUVECs with or without pre-miRs-125b, as described above.

In the tumor xenograft model, three million LLC cells were directly injected subcutaneously into the back flanks of 6-week-old female C57BL/6 mice. On days 10, 12, 14 and 17, we injected 400 pM control miR, pre-miR-125b or anti-miR-125b inhibitor (Applied Biosystems) using *in vivo*-jetPEI[26] (Polyplus Transfection, Illkirch, France) directly into the tumor mass. Measurements of tumor volume were performed as described previously.[35] Tumors were dissected for isolation of miRs and for immunofluorescence analysis 19 days after tumor cell inoculation.

Luciferase assays

The 3′UTR segments of human and mouse VE-Cadherin predicted to interact specifically with miR-125b were subcloned by standard procedures into the pMIR-REPORT Luciferase vector (Applied Biosystems) immediately downstream of the stop codon of the luciferase gene. In brief, we generated those oligos as follows: human VE-cadherin 3′UTR sense oligo (5′-CTAGTCCATGTGTCTTTACACCTCGCTGTTGTCACATCTCA GGGAACTGACCCTCAGGCACACCTGGATCCA-3′) ligated with the *Spe*1 site at the 3′ terminal and with *Bam*H1/*Hin*dIII at the 5′ terminal, and human VE-cadherin 3′UTR antisense oligo (5′-AGCTTGGATC CAGGTGTGCCTGAGGGTCAGTTCCCTGAGATGTGACAACAGCGAGGTGTAAA GACACATGGA-3′) ligated with the *Bam*H1/*Hin*dIII site at the 3′ terminal and with *Spe*1 at the 5′ terminal; human VE-cadherin 3′UTR mut (mutated sequences are underlined) sense oligo (5′-CTAGTCCATGTGTCTTTACA CCTCGCTGTTGTCACATCTTCAAACACTGACCCTCAGGCACACCTGGATCCA-3′) ligated with the *Spe*1 site at the 3′ terminal and with the *Bam*H1/*Hin*dIII at the 5′ terminal, and human VE-cadherin 3′UTR mut (mutated sequences underlined) antisense oligo (5′-AGCTTGGATCCAGGTGTGCCTGAGGGTCA GTGTTTGGAGATGTGACAACAGCGAGGTGTAAAGACACATGGA-3′) ligated with the *Bam*H1/*Hin*dIII site at the 3′ terminal and with the *Spe*1 at the 5′ terminal; mouse VE-cadherin 3′UTR sense oligo (5′-CTAGTCA CGCCACTCGCCTTTTGCCTAGTTGCCACATCTCAGGGAATGAACCTCACCCCCA GGGCGGATCCA-3′) ligated with the *Spe*1 site at the 3′ terminal and with the *Bam*H1/*Hin*d3 at the 5′ terminal, and mouse VE-cadherin 3′UTR antisense oligo (5′-AGCTTGGATCCGCCCTGGGGGTGAGGTTCATTCCCTGA GATGTGGCAACTAGGCAAAAGGCGAGTGGCGTGA-3′) ligated with the *Bam*H1/*Hin*dIII site at the 3′ terminal and with *Spe*1 at the 5′ terminal; mouse VE-cadherin 3′UTR mut (mutated sequences are underlined) sense oligo (5′-CTAGTCACGCCACTCGCCTTTTGCCTAGTTGCCACATCTTCAAACATG AACCTCACCCCCAGGGCGGATCCA-3′) ligated with the *Spe*1 site at the 3′ terminal and with the *Bam*H1/*Hin*dIII at the 5′ terminal, and mouse VE-cadherin 3′UTR mut (mutated sequences underlined) antisense oligo (5′-AGCTTGGATCCGCCCTGGGGGTGAGGTTCATGTTTGAAGATGTGGCAACT AGGCAAAAGGCGAGTGGCGTGA-3′) ligated with the *Bam*H1/*Hin*dIII site at the 3′ terminal and with *Spe*1 at the 5′ terminal. Double-stranded oligos were generated by annealing with sense and anti-sense oligos by standard methods and ligated into *Spe*1 and *Hin*dIII sites of the multiple cloning site of the pMIR-REPORT Luciferase vector. The vectors containing wild-type VE-cadherin or variant 3′UTR were transfected into HEK293 cells with or without miR-125b using Lipofectamine 2000. At 48 h after transfection, cells were lysed and luciferase activity was measured (POWERSCAN HT, DS Pharma Biomedical, Osaka, Japan). We used pMIR-REPORT β-gal control plasmid (Applied Biosystems) or pRL-TK plasmid (Promega, Madison, WI, USA) for normalization of luciferase values and the Dual-Glo Luciferase Assay System (Promega) for detection of luciferase activity.

Western blotting

Western blotting using anti-human VE-cadherin antibody was performed as previously described.[32] HUVECs were lysed 48 h after transfection with miR-125b or control miR.

Immunofluorescence

Tumor sections were stained with anti-mouse CD31 (Pharmingen, San Diego, CA, USA) and anti-mouse CD144 (VE-cadherin) antibody (BD Bioscience, San Diego, CA, USA). The procedure for tissue preparation and staining was as previously reported.[36] Lectin staining was performed as previously described[33] using fluorescein isothiocyanate-isolectin (Vector Lab, Burlingame, CA, USA). Hypoxic areas were identified by the fluorescein isothiocyanate-conjugated Hypoxyprobe-1 Mab1 (Natural Pharmacia International, Research Triangle Park, NC, USA). Samples were visualized using conventional microscopy (with a DM5500B equipped with HCX PL FLVOTAR 5/0.15 and HCX PL FLVOTAR 10/0.15 dry objective lenses; Leica, Solms, Germany) or confocal microscopy (Leica). Images were acquired with a DFC 500 digital camera (Leica) and processed with the Leica application suite (Leica) and Adobe Photoshop CS3 software (Adobe Systems, San Jose, CA, USA). All images shown are representative of 3–5 independent experiments.

Statistical analysis

All data were displayed as the mean s.d. and were analyzed by repeated-measures two-way analysis of variance or Student's *t*-test using Statview software (Abacus Concepts, Berkeley, CA, USA). A probability value of o 0.05 was considered statistically significant.

CONFLICT OF INTEREST

The authors declare no conflict of interest.

ACKNOWLEDGEMENTS

We thank S Fukuhara and N Mochizuki for supplying VE-cadherin expression plasmid, and K Fukuhara and N Fujimoto for technical assistance. This work was partly supported by a grant from the Ministry of Education, Science, Sports, and Culture of Japan.

REFERENCES

1 Risau W. Mechanisms of angiogenesis. *Nature* 1997; **386**: 671–674.
2 Dejana E. Endothelial adherens junctions: implications in the control of vascular permeability and angiogenesis. *J Clin Invest* 1996; **98**: 1949–1953.
3 Lindahl P, Johansson BR, Leveen P, Betsholtz C. Pericyte loss and microaneurysm formation in PDGF-B-deficient mice. *Science* 1997; **277**: 242–245.
4 Dumont DJ, Gradwohl G, Fong GH, Puri MC, Gertsenstein M, Auerbach A *et al.* Dominant-negative and targeted null mutations in the endothelial receptor tyrosine kinase, tek, reveal a critical role in vasculogenesis of the embryo. *Genes Dev* 1994; **8**: 1897–1909.
5 Sato TN, Tozawa Y, Deutsch U, Wolburg-Buchholz K, Fujiwara Y, Gendron-Maguire M *et al.* Distinct roles of the receptor tyrosine kinases Tie-1 and Tie-2 in blood vessel formation. *Nature* 1995; **376**: 70–74.
6 Suri C, Jones PF, Patan S, Bartunkova S, Maisonpierre PC, Davis S *et al.* Requisite role of angiopoietin-1, a ligand for the TIE2 receptor, during embryonic angiogenesis. *Cell* 1996; **87**: 1171–1180.
7 Augustin HG, Koh GY, Thurston G, Alitalo K. Control of vascular morphogenesis and homeostasis through the angiopoietin-Tie system. *Nat Rev Mol Cell Biol* 2009; **10**: 165–177.
8 Maisonpierre PC, Suri C, Jones PF, Bartunkova S, Wiegand SJ, Radziejewski C *et al.* Angiopoietin-2, a natural antagonist for Tie2 that disrupts in vivo angiogenesis. *Science* 1997; **277**: 55–60.
9 Vestweber D, Winderlich M, Cagna G, Nottebaum AF. Cell adhesion dynamics at endothelial junctions: VE-cadherin as a major player. *Trends Cell Biol* 2009; **19**: 8–15.
10 Dejana E, Tournier-Lasserve E, Weinstein BM. The control of vascular integrity by endothelial cell junctions: molecular basis and pathological implications. *Dev Cell* 2009; **16**: 209–221.

11 Gory-Faure S, Prandini MH, Pointu H, Roullot V, Pignot-Paintrand I, Vernet M *et al.* Role of vascular endothelial-cadherin in vascular morphogenesis. *Development* 1999; **126**: 2093-2102.
12 Carmeliet P, Lampugnani MG, Moons L, Breviario F, Compernolle V, Bono F *et al.* Targeted deficiency or cytosolic truncation of the VE-cadherin gene in mice impairs VEGF-mediated endothelial survival and angiogenesis. *Cell* 1999; **98**: 147-157.
13 Crosby CV, Fleming PA, Argraves WS, Corada M, Zanetta L, Dejana E *et al.* VE-cadherin is not required for the formation of nascent blood vessels but acts to prevent their disassembly. *Blood* 2005; **105**: 2771-2776.
14 Hendrix MJ, Seftor EA, Meltzer PS, Gardner LM, Hess AR, Kirschmann DA *et al.* Expression and functional significance of VE-cadherin in aggressive human melanoma cells: role in vasculogenic mimicry. *Proc Natl Acad Sci USA* 2001; **98**: 8018-8023.
15 Bartel DP. MicroRNAs: genomics, biogenesis, mechanism, and function. *Cell* 2004; **116**: 281-297.
16 Krek A, Grun D, Poy MN, Wolf R, Rosenberg L, Epstein EJ *et al.* Combinatorial microRNA target predictions. *Nat Genet* 2005; **37**: 495-500.
17 Suarez Y, Sessa WC. MicroRNAs as novel regulators of angiogenesis. *Circ Res* 2009; **104**: 442-454.
18 Wurdinger T, Tannous BA, Saydam O, Skog J, Grau S, Soutschek J *et al.* miR-296 regulates growth factor receptor overexpression in angiogenic endothelial cells. *Cancer Cell* 2008; **14**: 382-393.
19 Bonauer A, Carmona G, Iwasaki M, Mione M, Koyanagi M, Fischer A *et al.* MicroRNA-92a controls angiogenesis and functional recovery of ischemic tissues in mice. *Science* 2009; **324**: 1710-1713.
20 Kuehbacher A, Urbich C, Zeiher AM, Dimmeler S. Role of Dicer and Drosha for endothelial microRNA expression and angiogenesis. *Circ Res* 2007; **101**: 59-68.
21 Chen YH, Wu HL, Chen CK, Huang YH, Yang BC, Wu LW. Angiostatin antagonizes the action of VEGF-A in human endothelial cells via two distinct pathways. *Biochem Biophys Res Commun* 2003; **310**: 804-810.
22 Yamakuchi M, Lotterman CD, Bao C, Hruban RH, Karim B, Mendell JT *et al.* P53-induced microRNA-107 inhibits HIF-1 and tumor angiogenesis. *Proc Natl Acad Sci USA* 2010; **107**: 6334-6339.
23 Suzuki HI, Yamagata K, Sugimoto K, Iwamoto T, Kato S, Miyazono K. Modulation of microRNA processing by p53. *Nature* 2009; **460**: 529-533.
24 Scott GK, Goga A, Bhaumik D, Berger CE, Sullivan CS, Benz CC. Coordinate suppression of ERBB2 and ERBB3 by enforced expression of micro-RNA miR-125a or miR-125b. *J Biol Chem* 2007; **282**: 1479-1486.
25 Shi XB, Xue L, Yang J, Ma AH, Zhao J, Xu M *et al.* An androgen-regulated miRNA suppresses Bak1 expression and induces androgen-independent growth of prostate cancer cells. *Proc Natl Acad Sci USA* 2007; **104**: 19983-19988.
26 Niola F, Evangelisti C, Campagnolo L, Massalini S, Bue MC, Mangiola A *et al.* A plasmid-encoded VEGF siRNA reduces glioblastoma angiogenesis and its combination with interleukin-4 blocks tumor growth in a xenograft mouse model. *Cancer Biol Ther* 2006; **5**: 174-179.
27 Okamoto R, Ueno M, Yamada Y, Takahashi N, Sano H, Suda T *et al.* Hematopoietic cells regulate the angiogenic switch during tumorigenesis. *Blood* 2005; **105**: 2757-2763.
28 Takakura N. Role of hematopoietic lineage cells as accessory components in blood vessel formation. *Cancer Sci* 2006; **97**: 568-574.
29 Baumer S, Keller L, Holtmann A, Funke R, August B, Gamp A *et al.* Vascular endothelial cell-specific phosphotyrosine phosphatase (VE-PTP) activity is required for blood vessel development. *Blood* 2006; **107**: 4754-4762.
30 Gotsch U, Borges E, Bosse R, Boggemeyer E, Simon M, Mossmann H *et al.* VE-cadherin antibody accelerates neutrophil recruitment in vivo. *J Cell Sci* 1997; **110** (Pt 5): 583-588.
31 Holash J, Maisonpierre PC, Compton D, Boland P, Alexander CR, Zagzag D *et al.* Vessel cooption, regression, and growth in tumors mediated by angiopoietins and VEGF. *Science* 1999; **284**: 1994-1998.
32 Kidoya H, Ueno M, Yamada Y, Mochizuki N, Nakata M, Yano T *et al.* Spatial and temporal role of the apelin/APJ system in the caliber size regulation of blood vessels during angiogenesis. *EMBO J* 2008; **27**: 522-534.
33 Yamada Y, Takakura N. Physiological pathway of differentiation of hematopoietic stem cell population into mural cells. *J Exp Med* 2006; **203**: 1055-1965.
34 Kidoya H, Kunii N, Naito H, Muramatsu F, Okamoto Y, Nakayama T *et al.* The apelin/APJ system induces maturation of the tumor vasculature and improves the efficiency of immune therapy. *Oncogene* 2012; **31**: 3254-3264.
35 Nagahama Y, Ueno M, Miyamoto S, Morii E, Minami T, Mochizuki N *et al.* PSF1, a DNA replication factor expressed widely in stem and progenitor cells, drives tumorigenic and metastatic properties. *Cancer Res* 2010; **70**: 1215-1224.
36 Takakura N, Watanabe T, Suenobu S, Yamada Y, Noda T, Ito Y *et al.* A role for hematopoietic stem cells in promoting angiogenesis. *Cell* 2000; **102**: 199-209.

Supplementary Information accompanies the paper on the Oncogene website (http://www.nature.com/onc)

LETTER

doi:10.1038/nature11930

Critical role of Trib1 in differentiation of tissue-resident M2-like macrophages

Takashi Satoh[1,2], Hiroyasu Kidoya[3], Hisamichi Naito[3], Masahiro Yamamoto[4,5], Naoki Takemura[1,2], Katsuhiro Nakagawa[1,2], Yoshichika Yoshioka[6], Eiichi Morii[7], Nobuyuki Takakura[3], Osamu Takeuchi[1,2,8] & Shizuo Akira[1,2]

Macrophages consist of at least two subgroups, M1 and M2 (refs 1–3). Whereas M1 macrophages are proinflammatory and have a central role in host defence against bacterial and viral infections[4,5], M2 macrophages are associated with responses to anti-inflammatory reactions, helminth infection, tissue remodelling, fibrosis and tumour progression[6]. Trib1 is an adaptor protein involved in protein degradation by interacting with COP1 ubiquitin ligase[7]. Genome-wide association studies in humans have implicated TRIB1 in lipid metabolism[8–10]. Here we show that Trib1 is critical for the differentiation of F4/80$^+$MR$^+$ tissue-resident macrophages—that share characteristics with M2 macrophages (which we term M2-like macrophages)—and eosinophils but not for the differentiation of M1 myeloid cells. Trib1 deficiency results in a severe reduction of M2-like macrophages in various organs, including bone marrow, spleen, lung and adipose tissues. Aberrant expression of C/EBPα in Trib1-deficient bone marrow cells is responsible for the defects in macrophage differentiation. Unexpectedly, mice lacking Trib1 in haematopoietic cells show diminished adipose tissue mass accompanied by evidence of increased lipolysis, even when fed a normal diet. Supplementation of M2-like macrophages rescues the pathophysiology, indicating that a lack of these macrophages is the cause of lipolysis. In response to a high-fat diet, mice lacking Trib1 in haematopoietic cells develop hypertriglyceridaemia and insulin resistance, together with increased proinflammatory cytokine gene induction. Collectively, these results demonstrate that Trib1 is critical for adipose tissue maintenance and suppression of metabolic disorders by controlling the differentiation of tissue-resident M2-like macrophages.

Members of the tribble family are pseudokinase proteins that are conserved among species and implicated in various human diseases, such as leukaemia and metabolic disorders. Tribble proteins interact with an E3 ubiquitin ligase, COP1, for protein degradation. In thioglycollate-elicited macrophages, Trib1 is important for interleukin (IL)-12p40 production to lipopolysaccharide[11]. In addition, Trib1 and Trib2 have been implicated in acute myeloid leukaemia[12,13]. Trib3 can inhibit insulin signalling[14], although *Trib3*$^{-/-}$ mice do not show defects in insulin signalling or glucose homeostasis[15]. However, the roles of tribble proteins in haematopoietic cell development have not been clarified.

First, we examined the populations of tissue-resident macrophages in mice lacking tribble family genes in the spleen. Although the proportions of B cells, T cells, dendritic cells and Ly6C^{high}Mac1$^+$ inflammatory monocytes were not altered between wild-type and *Trib1*$^{-/-}$ splenocytes, F4/80$^+$Mac1$^+$ macrophages, which also expressed Mrc1 (also called MR), *Arg1* and *Fizz1* (also called *Retnla*), were markedly reduced and Siglec-F$^+$CCR3$^+$ eosinophils were absent in *Trib1*$^{-/-}$ spleens (Fig. 1a and Supplementary Figs 1 and 2). In contrast, the neutrophil population was increased in *Trib1*$^{-/-}$ spleens (Fig. 1a and Supplementary Fig. 3). Splenic F4/80$^+$ red pulp macrophages phagocytose aged red blood cells and accumulate iron[16,17]. Immunohistochemical staining of spleen sections confirmed the absence of red pulp macrophages in *Trib1*$^{-/-}$ spleen (Fig. 1b). Furthermore, Perl's Prussian blue staining of the spleen sections revealed that iron did not accumulate in *Trib1*$^{-/-}$ mice (Fig. 1c and Supplementary Fig. 4). In contrast, splenic metallophilic and marginal zone macrophages were normal in *Trib1*$^{-/-}$ mice (Supplementary Fig. 5). In addition to the spleen, tissue-resident macrophages in other tissues were severely decreased in *Trib1*$^{-/-}$ mice; however, peritoneal resident macrophages were comparable between wild-type and *Trib1*$^{-/-}$ mice (Supplementary Fig. 6). Newly generated *Trib2*$^{-/-}$ and *Trib3*$^{-/-}$ mice did not show any defects in myeloid and lymphoid cells in the spleen (Supplementary Figs 7 and 8). Because MR, Arg1 and Fizz1 expression is a hallmark characteristic of M2 macrophages, we termed this population M2-like macrophages. Thus, these findings indicate that Trib1 is critical for the differentiation of tissue-resident M2-like macrophages and eosinophils in the peripheral organs.

Differentiation of haematopoietic cells, including macrophages, occurs in the bone marrow, followed by their migration to peripheral tissues via the bloodstream. Consistent with the defects observed in peripheral organs, numbers of F4/80$^+$Mac1$^+$ cells and Siglec-F$^+$CCR3$^+$ eosinophils were severely decreased in the blood and bone marrow cells from *Trib1*$^{-/-}$ mice whereas numbers of Gr-1^{high} neutrophils were slightly increased (Fig. 1d, e). However, inflammatory monocytes were comparable between wild-type and *Trib1*$^{-/-}$ bone marrow cells (Supplementary Fig. 9). The adoptive transfer of *Trib1*$^{-/-}$ bone marrow cells to wild-type mice failed to increase F4/80$^+$ macrophage numbers in the bone marrow and spleen (data not shown). Furthermore, competitive transfer of CD45.1$^+$ wild-type and CD45.2$^+$ *Trib1*$^{-/-}$ bone marrow cells (1:1 ratio) to sublethal-irradiated wild-type mice led to severely impaired development of CD45.2$^+$ macrophages and eosinophils, and increased the population of neutrophils (Supplementary Fig. 10). These findings demonstrate that the defects observed in *Trib1*$^{-/-}$ mice are intrinsic to haematopoietic cells, and that Trib1 is critical for regulating the proper differentiation of myeloid cells in the bone marrow. To delineate the developmental competency of *Trib1*$^{-/-}$ bone marrow cells, we performed colony-forming assays. Whereas granulocyte/neutrophil colonies were increased, macrophage colonies were severely decreased and eosinophil colonies were not generated in *Trib1*$^{-/-}$ bone marrow cells compared with wild-type cells (Fig. 2a). We found that macrophage colonies could be morphologically classified into two subgroups, namely aggregated/small and diffused/large macrophages (Fig. 2b). Although most wild-type macrophage colonies were aggregated and small, the macrophage colonies obtained from *Trib1*$^{-/-}$ bone marrow cells were diffused and large (Fig. 2b). These results indicated that Trib1 is essential for the proper

[1]Laboratory of Host Defense, WPI Immunology Frontier Research Center (WPI IFReC), Osaka University, 3-1 Yamada-oka, Suita, Osaka 565-0871, Japan. [2]Department of Host Defense, Research Institute for Microbial Diseases (RIMD), Osaka University, 3-1 Yamada-oka, Suita, Osaka 565-0871, Japan. [3]Department of Signal Transduction, Research Institute for Microbial Diseases (RIMD), Osaka University, 3-1 Yamada-oka, Suita, Osaka 565-0871, Japan. [4]Laboratory of immunoparasitology, WPI Immunology Frontier Research Center (WPI IFReC), Osaka University, 3-1 Yamada-oka, Suita, Osaka 565-0871, Japan. [5]Department of Immunoparasitology, Research Institute for Microbial Diseases (RIMD), Osaka University, 3-1 Yamada-oka, Suita, Osaka 565-0871, Japan. [6]Laboratory of Biofunctional Imaging, WPI Immunology Frontier Research Center (WPI IFReC), Osaka University, 3-1 Yamada-oka, Suita, Osaka 565-0871, Japan. [7]Department of Pathology, Graduate School of Medicine, Osaka University, 2-2 Yamada-oka, Suita, Osaka 565-0871, Japan. [8]Laboratory of Infection and Prevention, Institute for Virus Research, Kyoto University, 53 Shogoin Kawara-cho, Sakyo-ku, Kyoto 606-8507, Japan.

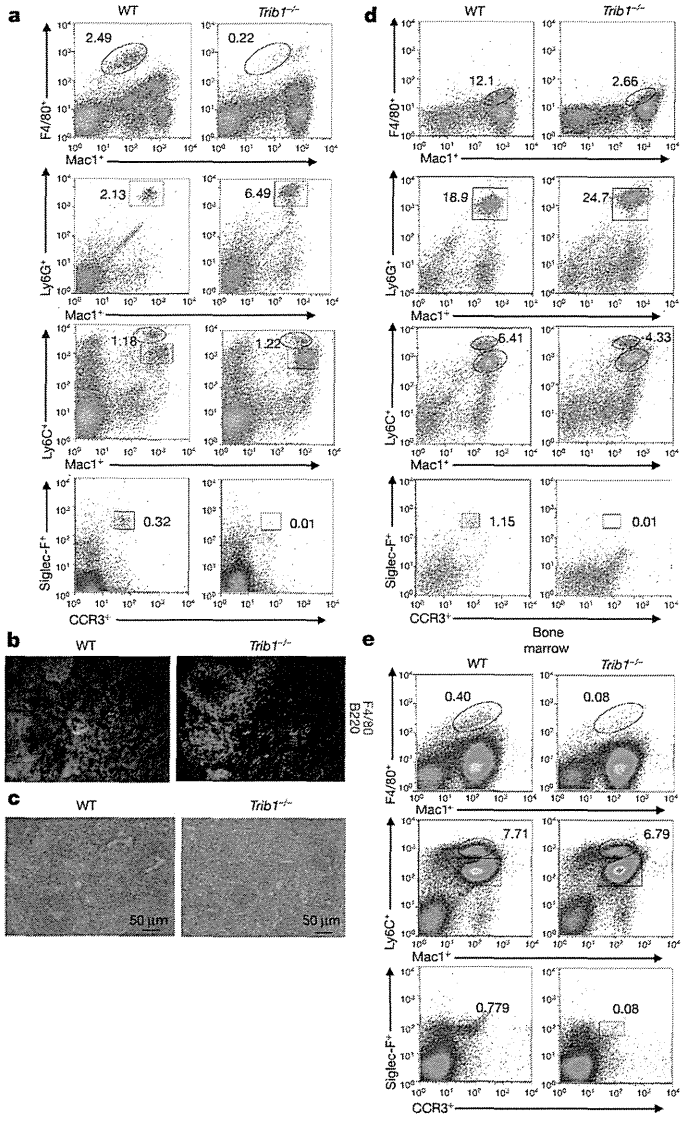

Figure 1 | Lack of tissue-resident M2-like macrophages and eosinophils in *Trib1*-deficient mice. **a**, Flow cytometric analyses of splenocytes. The expression levels of F4/80$^+$ and Mac1$^+$ tissue-resident M2-like macrophages in splenocytes are shown (top). The proportions of inflammatory monocytes and neutrophils (middle) and eosinophils (bottom) in splenocytes are also shown. Similar results were obtained in eight independent experiments. **b**, Wild-type (WT) and *Trib1*$^{-/-}$ spleen sections were stained for F4/80 (red) and B220 (green). **c**, Images of Perl's Prussian blue staining for ferric iron in the spleens of wild-type and *Trib1*$^{-/-}$ mice. Scale bars, 50 μm. **d**, Flow cytometric analysis of cell populations in the blood. The percentages of F4/80$^+$ and Mac1$^+$ cells in the blood are shown. **e**, Flow cytometric analysis of bone marrow. The percentages of F4/80$^+$ and Mac1$^+$ tissue-resident M2-like macrophages in the bone marrow are shown (top). The proportions of inflammatory monocytes and neutrophils (middle) and eosinophils (bottom) in the bone marrow are also shown. Similar results were obtained in three independent experiments (**b**–**e**).

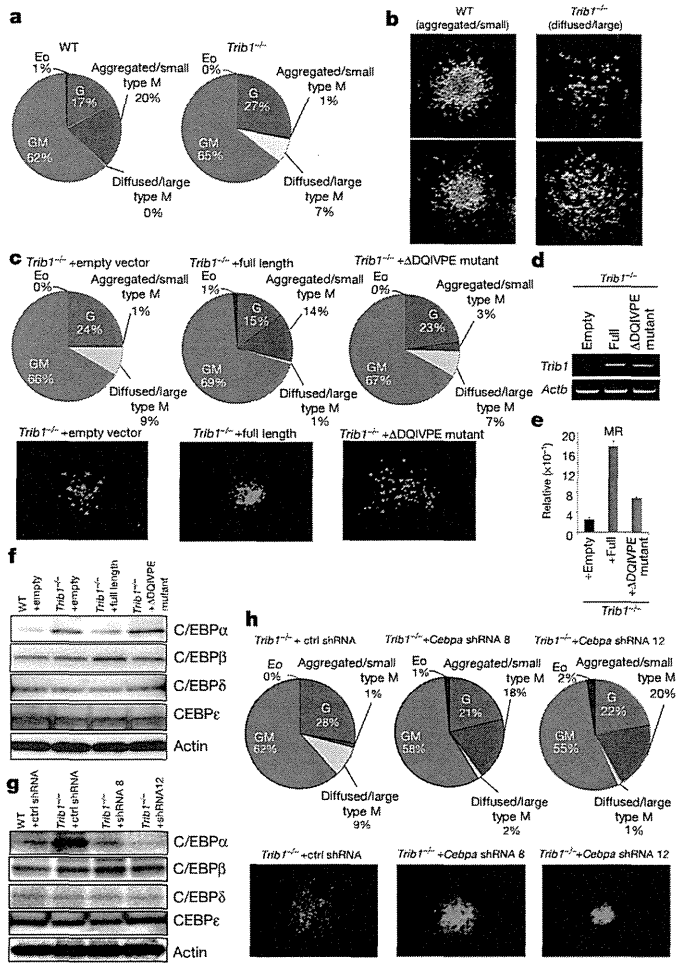

Figure 2 | Trib1 controls macrophage, eosinophil and neutrophil differentiation via the ubiquitin-binding domain. **a**, **b**, Bone marrow cells were subjected to colony-forming assays. Each colony was counted depending on the morphology (**a**), and images of the cell types of macrophage colonies are shown (**b**). Eo, eosinophil colonies; G, granulocyte/neutrophil colonies; GM, granulocyte/macrophage colonies; M, macrophage colonies. **c**–**e**, Role of the COP1-binding site in macrophage differentiation. Bone marrow cells lacking *Trib1* were infected with retroviruses expressing empty vector, full-length Trib1 (mTrib1) or Trib1(ΔDQIVPE) mutant. Colony-forming assays were performed in retrovirus-infected (GFP$^+$) cells. Images of the retrovirus-infected (GFP$^+$) cell types of macrophage colonies are shown in **c**. **d**, Semi-quantitative PCR analyses were performed to measure the expression of *Trib1* in empty vector, full-length Trib1 (full length) or mutant Trib1(ΔDQIVPE) in macrophage colonies. **e**, Quantitative PCR analyses were performed for MR expression in macrophage colonies expressing empty vector, Trib1 (full length) or mutant Trib1(ΔDQIVPE). Error bars indicate s.d. of duplicates. Similar results were obtained in three independent experiments (**a**–**e**). **f**, Immunoblot analyses of various C/EBP family molecules. Lineage-negative fractions from wild-type, *Trib1*$^{-/-}$ cells, *Trib1*$^{-/-}$ cells expressing full-length and *Trib1*$^{-/-}$ cells expressing mutant Trib1(ΔDQIVPE) were analysed by western blotting. **g**, **h**, Role of C/EBPα in macrophage differentiation. Bone marrow cells lacking *Trib1* were infected with retroviruses expressing empty vector, *Cebpa* shRNA 8 or *Cebpa* shRNA 12. Immunoblot analyses of various C/EBP family molecules. Lineage-negative fractions from wild-type, *Trib1*$^{-/-}$ cells and *Trib1*$^{-/-}$ cells expressing *Cebpa* shRNA 8 or *Cebpa* shRNA 12 were analysed by western blotting (**g**). Colony-forming assays were performed in infected (GFP$^+$) cells, and images of the retrovirus-infected (GFP$^+$) cell types of macrophage colonies are shown (**h**). Similar results were obtained in two independent experiments (**f**–**h**).

differentiation of bone marrow myeloid cells. Proportions of CMP and CLP as well as GMP were comparable between wild-type and *Trib1*$^{-/-}$ mice (see Supplementary Fig. 11 for definitions). Furthermore, the expression pattern of transcriptional factors, which are involved in myeloid cell differentiation, in GMP and MDP was also comparable between wild-type and *Trib1*$^{-/-}$ mice (Supplementary Fig. 12), suggesting that Trib1 controls myeloid cell differentiation downstream of GMP.

Retroviral expression of full-length Trib1 in *Trib1*$^{-/-}$ bone marrow cells resulted in a marked increase in aggregated and small macrophage colonies and eosinophil colonies, but decreased granulocyte/neutrophil colonies (Fig. 2c, d and Supplementary Fig. 13). In contrast, expression of Trib1 lacking the COP1-binding site (Trib1(ΔDQIVPE) mutant) in *Trib1*$^{-/-}$ bone marrow cells failed to restore the differentiation defects. Moreover, expression of full-length Trib1, but not of

Trib1(ΔDQIVPE) mutant, restored expression of M2 macrophage marker genes such as *MR* (Fig. 2e). Next, we investigated the expression of potential target proteins of the Trib1–COP1 axis in *Trib1*$^{-/-}$ bone marrow cells. Among the transcription factors, C/EBP family members are important for determining the balance between granulopoiesis and monopoiesis[18]. We found that expression of C/EBPα, but not other transcriptional factors involved in myeloid cell differentiation, was increased in lineage-negative bone marrow cells and macrophage colonies lacking Trib1 (Fig. 2f and Supplementary Fig. 14). The expression of full-length Trib1 in *Trib1*$^{-/-}$ bone marrow cells suppressed the level of C/EBPα expression (Fig. 2f). To address whether increased expression of C/EBPα is involved in aberrant myeloid cell differentiation under Trib1 deficiency, we genetically inhibited *Cebpa* in *Trib1*$^{-/-}$ bone marrow cells using short hairpin RNAs (shRNAs) (Supplementary Fig. 15). The decreased C/EBPα protein expression in *Trib1*$^{-/-}$ bone marrow cells was similar to levels of

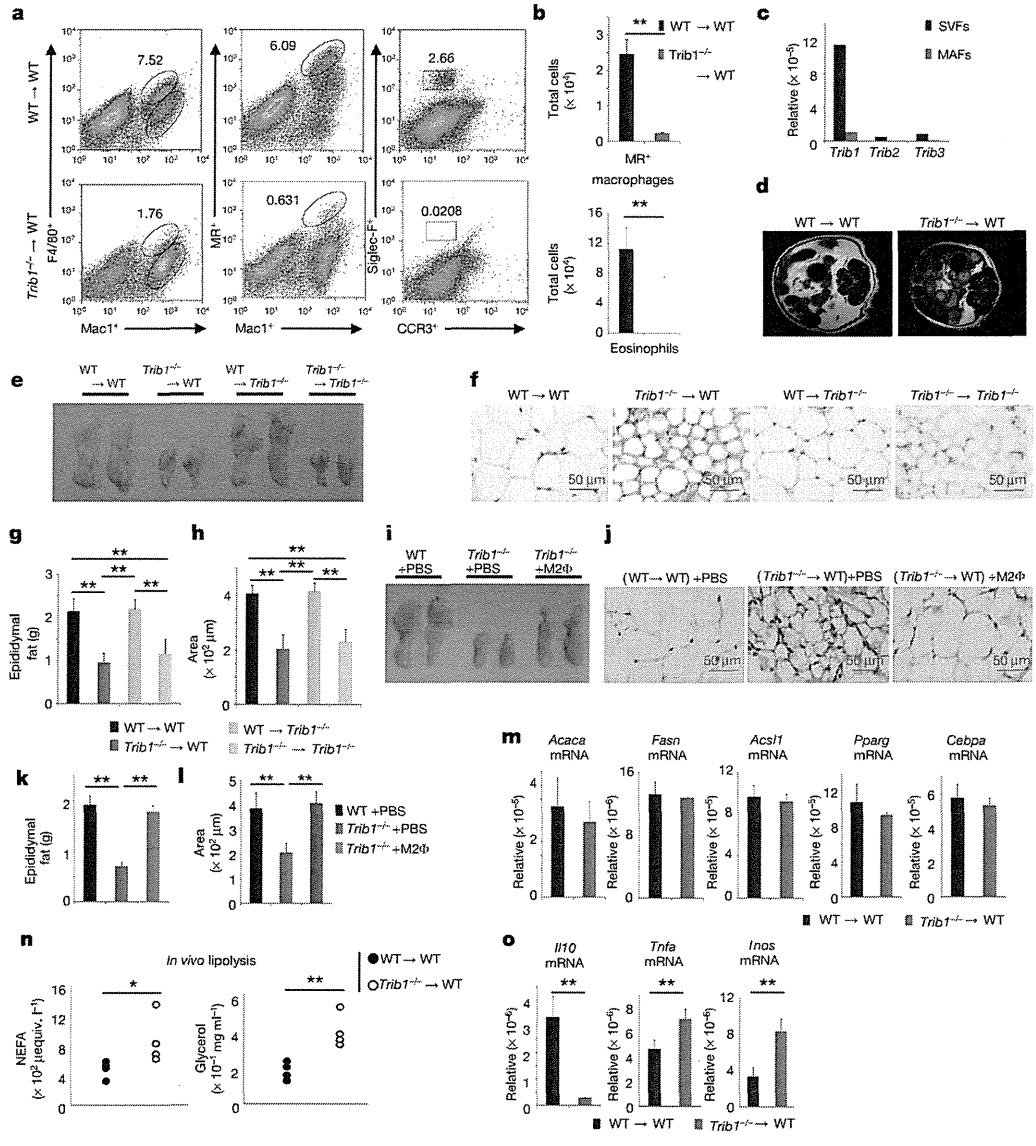

Figure 3 | Impact of Trib1 deficiency on lipodystrophy. **a**, **b**, Flow cytometric analyses of haematopoietic cells in adipose tissue. The expression levels of F4/80^{+} and Mac1^{+} or MR^{+} and Mac1^{+} tissue-resident M2 macrophages in adipose tissue (left and centre) and Siglec-F^{+} and CCR3^{+} eosinophils (right) are shown. The total numbers of MR^{+} macrophages and eosinophils in adipose tissues from wild-type and *Trib1*$^{-/-}$ chimaeric mice fed a normal diet are shown (**b**). Error bars indicate s.d. of duplicates. Similar results were obtained in three independent experiments. **c**, Expression levels of *Trib1*, *Trib2* and *Trib3* in SVFs and MAFs, assessed by quantitative PCR. Similar results were obtained in two independent experiments. **d**, The epididymal adipose tissues from wild-type and *Trib1*$^{-/-}$ chimaeric mice fed a normal diet were analysed by magnetic resonance imaging (MRI). **e**, Images of the epididymal adipose tissues from each indicated chimaeric mice fed a normal diet are shown. **f**, Haematoxylin and eosin-stained images of paraffin-embedded epididymal adipose tissue sections from each indicated chimaeric mice fed a normal diet. Scale bars, 50 μm. **g**, **h**, The total epididymal fat weight was measured (**g**) and each area of adipocytes was measured (**h**) in each indicated chimaeric mouse. Error bars indicate s.d. of duplicates. **i**, Images of the epididymal adipose tissues from each indicated chimaeric mice fed a normal diet are shown. **j**, Haematoxylin-and-eosin-stained images of paraffin-embedded epididymal adipose tissue sections from each indicated chimaeric mice fed a normal diet. Scale bars, 50 μm. **k**, **l**, The total epididymal fat weight (**k**) and each area of adipocytes were measured (**l**) in each indicated chimaeric mouse. **m**, Total RNA was prepared from wild-type and *Trib1*$^{-/-}$ chimaeric mice fed a normal diet. The expression levels of mRNAs encoding the indicated proteins were determined by quantitative PCR. Error bars indicate s.d. of duplicates. Similar results were obtained in three independent experiments (**e**–**m**). **n**, Lipolysis assays in wild-type and *Trib1*$^{-/-}$ mice fed a normal diet. The serum glycerol and NEFA levels were measured *in vivo*. Similar results were obtained in two independent experiments. **o**, Total RNA was prepared from wild-type and *Trib1*$^{-/-}$ chimaeric mice fed a normal diet. The expression levels of mRNAs encoding the indicated proteins were determined by quantitative PCR. Error bars indicate s.d. of duplicates. Similar results were obtained in three independent experiments. Statistical significance in **b**, **g**, **h**, **k**, **l**, **n**, **o** was determined using the Student's *t*-test. $^{*}P < 0.05$; $^{**}P < 0.01$.

wild-type cells (Fig. 2g). Repression of *Cebpa* resulted in an increase in the aggregated and small macrophage colonies and eosinophil colonies, but a decrease in granulocyte/neutrophil colonies (Fig. 2h). Taken together, these data demonstrate that Trib1 regulates myeloid cell differentiation by altering the expression of C/EBPα in a COP1-dependent manner.

Recent genome-wide association studies revealed that genetic variants in the loci corresponding to *TRIB1* are associated with increased plasma lipoprotein concentrations, a high risk of ischaemic heart disease and myocardial infarction in humans[8–10]. These studies prompted us to investigate the role of Trib1 in the adipose tissue and liver of mice. Because we did not observe histological changes in the liver in the absence of Trib1 in mice fed normal chow (Supplementary Fig. 16), we next examined the adipose tissues. Consistent with observations in other organs, $MR^+F4/80^+$ adipose-tissue-resident M2-like macrophages were severely decreased in the stromal vascular fraction (SVF) derived from *Trib1*$^{-/-}$ epididymal adipose tissues compared with wild-type mice (Supplementary Fig. 17). Mice lacking Trib1 in haematopoietic cells also showed a reduced number of M2-like macrophages and lacked eosinophils in epididymal adipose tissues (Fig. 3a, b), and *Trib1* mRNA was rarely expressed in the normal mature adipocyte fraction (MAF) (Fig. 3c), indicating that the defect is intrinsic to haematopoietic cells. In contrast, $CD11c^+Mac1^+$ M1 macrophages were hardly present in wild-type and *Trib1*$^{-/-}$ adipose tissues from mice fed a normal chow diet (Supplementary Fig. 17). Unexpectedly, MRI analyses revealed that Trib1 deficiency in haematopoietic cells severely reduced the abdominal adipose tissues (Fig. 3d). The epididymal adipose tissues and size of each epididymal adipocyte were significantly smaller in mice lacking Trib1 in all tissues as well as in haematopoietic cells only, than in littermate wild-type mice fed a normal diet (Fig. 3e–h). Thus, the mice showed a lipodystrophic phenotype. In contrast, *Trib1*$^{-/-}$ mice harbouring wild-type haematopoietic cells did not develop lipodystrophy (Fig. 3e, f). These findings demonstrate that Trib1 deficiency in haematopoietic cells is responsible for development of this pathophysiology. To investigate whether loss of M2-like macrophages is responsible for the development of lipodystrophy, we supplemented *Trib1*$^{-/-}$ mice with these macrophages (Supplementary Fig. 18). After 3 weeks, the epididymal adipose tissues and the size of each adipocyte from *Trib1*$^{-/-}$ mice reconstituted with these macrophages were significantly larger than in PBS-treated *Trib1*$^{-/-}$ mice (Fig. 3i–l). Collectively, these data indicate that lack of M2-like macrophages, caused by Trib1 deficiency, is important for the development of the lipodystrophic phenotype.

Next, we examined the mechanisms of the lipodystrophy caused by Trib1 deficiency in haematopoietic cells. Adipose tissues are maintained by balance between lipogenesis and lipolysis. The mRNA levels of genes involved in adipocyte differentiation and lipogenesis were comparable between wild-type and *Trib1*$^{-/-}$ bone marrow chimaeric mice (Fig. 3m and Supplementary Fig. 19; see Methods). In contrast, the serum levels of non-esterified fatty acids (NEFAs) and glycerol were significantly elevated in *Trib1*$^{-/-}$ bone marrow chimaeric mice (Fig. 3n), indicative of enhanced lipolysis caused by Trib1 deficiency. Cytokines produced by macrophages contribute to adipose tissue inflammation and lipolysis. Expression of IL-10 was severely reduced in epididymal adipose tissues lacking Trib1 in haematopoietic cells. In contrast, *Tnf* and *Inos* mRNA expression were elevated in adipose tissues from *Trib1*$^{-/-}$ bone marrow chimaeric mice (Fig. 3o). Because several reports indicated that IL-10 has a central role in repressing lipolysis in adipocytes in addition to having anti-inflammatory effects[19–21], it is possible that M2-like macrophages are important for maintaining adipose tissues, at least in part, through the production of IL-10. However, the contribution of additional molecules produced by the macrophages may also be critical for amelioration of lipodystrophy.

Lipodystrophy is often associated with metabolic abnormalities. Although significant differences in levels of the parameters such as serum glucose, cholesterol, triglyceride and insulin were not detected between wild-type and *Trib1*$^{-/-}$ bone marrow chimaeric mice fed a normal diet, the feeding of mice with a high-fat diet (HFD) led to much higher elevations of these parameters in the serum of *Trib1*$^{-/-}$ bone marrow chimaeric mice (Fig. 4a). Mice lacking Trib1 throughout the whole body and in haematopoietic cells also developed glucose intolerance and insulin resistance on a HFD (Fig. 4b, c and Supplementary Fig. 20). In contrast, body weight did not differ significantly between wild-type and *Trib1*$^{-/-}$ bone marrow chimaeric mice fed a HFD (Supplementary Fig. 21). Whereas numbers of M1-type macrophages increased in both wild-type and *Trib1*$^{-/-}$ bone marrow chimaeric mice as well as mice lacking Trib1 in the whole body fed a HFD,

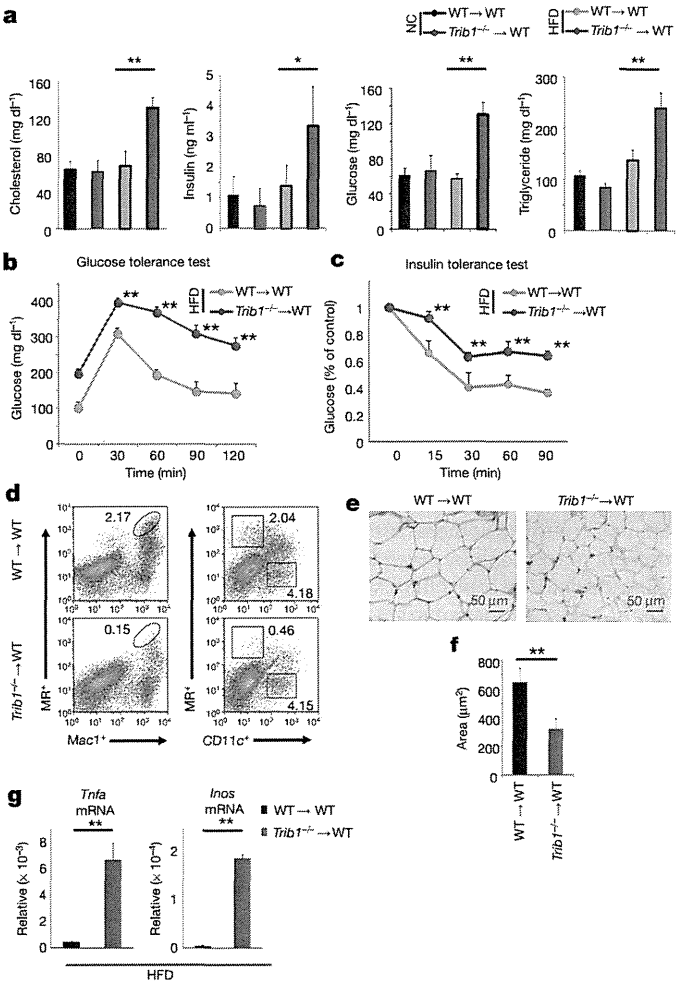

Figure 4 | Mice lacking Trib1 in haematopoietic cells develop exacerbated metabolic disorders on a high-fat diet. **a**, Serum samples were obtained from bone-marrow-transferred wild-type and *Trib1*$^{-/-}$ littermates fed normal chow (NC) or a high-fat diet (HFD). The concentrations of cholesterol, insulin, glucose and triglyceride were measured. Error bars indicate s.d. of duplicates. **b**, **c**, Fasting male bone-marrow-transferred wild-type and *Trib1*$^{-/-}$ littermates fed a HFD were challenged with intraperitoneal glucose (**b**) or insulin (**c**), and blood was sampled for glucose analyses at the indicated times. Data are mean s.d. of 5 samples. **d**, Flow cytometric analyses of haematopoietic cells from adipose tissues in wild-type and *Trib1*$^{-/-}$ mice fed a HFD. The expression levels of MR^+ and $Mac1^+$ tissue-resident macrophages are shown (left). The MR^+ and $CD11c^+$ macrophages in adipose tissue are also shown (right). **e**, **f**, Haematoxylin-and-eosin-stained images of paraffin-embedded epididymal adipose tissue sections are shown (**e**), and each area of adipocytes was measured (**f**). Scale bars, 50 μm. **g**, Total RNA was prepared from wild-type and *Trib1*$^{-/-}$ chimaeric mice fed a HFD. Error bars indicate s.d. of duplicates. The expression levels of mRNAs encoding the indicated genes were determined by quantitative PCR. Error bars indicate s.d. of duplicates. Statistical significance in **a**–**c**, **f**, **g** was determined using the Student's *t*-test. $*P < 0.05$; $**P < 0.01$.

M2-like macrophages were severely decreased in the absence of Trib1 (Fig. 4d and Supplementary Fig. 22). *Trib1*$^{-/-}$ chimaeric mice had smaller adipocytes on a HFD (Fig. 4e, f). Notably, *Tnf* and *Inos* mRNA were markedly augmented in *Trib1*$^{-/-}$ chimaeric mice (Fig. 4g). Taken together, these findings suggest that *Trib1*$^{-/-}$ bone marrow chimaeric mice develop metabolic disorders on a HFD through impaired lipid buffering caused by lipodystrophy.

Although we previously showed that Trib1 regulates C/EBPβ expression in thioglycollate-elicited macrophages[11], we found that M2-like macrophages were present in *Cebpb*$^{-/-}$ mice (data not shown). Thus, Trib1 seems to control different target proteins for degradation depending on the cell types and their differentiation stages. We previously showed that Jmjd3 is essential for M2-like macrophage differentiation in response to chitin administration and helminth infection[22,23]. However, Jmjd3 deficiency did not show any defect in tissue-resident M2-like macrophage generation (Supplementary Fig. 23). Reciprocally, Trib1 deficiency did not alter the activation of M2-like macrophages to chitin administration (Supplementary Fig. 24). It can be assumed that macrophage subtypes are more complex *in vivo*, although the precise classification of M2-type macrophages *in vivo* is yet to be clarified.

Chronic low-grade inflammation in adipose tissues is thought to have a central role in the exacerbation of metabolic disorders[24,25]. M1-type macrophages infiltrate into obese adipose tissues via MCP1, where they are activated in part by saturated fatty acids and cause low-grade inflammation by producing proinflammatory cytokines[26,27]. However, tissue-resident M2-like macrophages, which differentiate depending on the presence of Trib1 in the bone marrow, are subsequently activated in adipose tissues and the liver in response to IL-4 and IL-13 produced from eosinophils by a PPAR-γ- and PPAR-δ-dependent mechanism, respectively[21,28–30]. Further studies are required to clarify how tissue-resident M2-like macrophages maintain adipose tissue homeostasis. Trib1 was also essential for the development of eosinophils, nevertheless, we believe that Trib1 maintains adipose tissues by controlling M2-like macrophages, as supplementation of wild-type macrophages alone could rescue the lipodystrophy observed in *Trib1*$^{-/-}$ mice.

Mutations in TRIB1 have been implicated in metabolic disorders of humans. It is tempting to speculate that TRIB1 functions in a similar manner in humans and that other pathophysiologies, such as tumour progression, angiogenesis or tissue remodelling, are affected by these tissue-resident M2-like macrophages.

METHODS SUMMARY

Mice, reagents, cells and plasmids. Full details are provided in the Methods.

Colony-forming assay. Bone marrow cells (4×10^4) were seeded on 3.5-cm dishes and cultured for 7 days with Methocult (no. 3534; Stem Cell Technologies) containing SCF, IL-6 and IL-3 in the presence of 20 ng ml^{-1} M-CSF. The numbers of GFP-positive cells were counted for colony-forming assays or collected for real-time (q)PCR and western blotting.

Full Methods and any associated references are available in the online version of the paper.

Received 19 March 2012; accepted 22 January 2013.
Published online 20 March 2013.

1. Martinez, F. O., Helming, L. & Gordon, S. Alternative activation of macrophages: an immunologic functional perspective. *Annu. Rev. Immunol.* **27,** 451–483 (2009).
2. Biswas, S. K. & Mantovani, A. Macrophage plasticity and interaction with lymphocyte subsets: cancer as a paradigm. *Nature Immunol.* **11,** 889–896 (2010).
3. Mantovani, A. & Sica, A. Macrophages, innate immunity and cancer: balance, tolerance, and diversity. *Curr. Opin. Immunol.* **22,** 231–237 (2010).
4. Takeuchi, O. & Akira, S. Pattern recognition receptors and inflammation. *Cell* **140,** 805–820 (2010).
5. Medzhitov, R. Origin and physiological roles of inflammation. *Nature* **454,** 428–435 (2008).
6. Sica, A. & Mantovani, A. Macrophage plasticity and polarization: *in vivo* veritas. *J. Clin. Invest.* **122,** 787–795 (2012).
7. Yokoyama, T. *et al.* Trib1 links the MEK1/ERK pathway in myeloid leukemogenesis. *Blood* **116,** 2768–2775 (2010).
8. Varbo, A., Benn, M., Tybjaerg-Hansen, A., Grande, P. & Nordestgaard, B. G. TRIB1 and GCKR polymorphisms, lipid levels, and risk of ischemic heart disease in the general population. *Arterioscler. Thromb. Vasc. Biol.* **31,** 451–457 (2011).
9. Aung, L. H. *et al.* Association of the TRIB1 tribbles homolog 1 gene rs17321515 A>G polymorphism and serum lipid levels in the Mulao and Han populations. *Lipids Health Dis.* **10,** 230 (2011).
10. Chambers, J. C. *et al.* Genome-wide association study identifies loci influencing concentrations of liver enzymes in plasma. *Nature Genet.* **43,** 1131–1138 (2011).
11. Yamamoto, M. *et al.* Enhanced TLR-mediated NF-IL6 dependent gene expression by Trib1 deficiency. *J. Exp. Med.* **204,** 2233–2239 (2007).
12. Jin, G. *et al.* Trib1 and Evi1 cooperate with Hoxa and Meis1 in myeloid leukemogenesis. *Blood* **109,** 3998–4005 (2007).
13. Keeshan, K. *et al.* Tribbles homolog 2 inactivates C/EBPα and causes acute myelogenous leukemia. *Cancer Cell* **10,** 401–411 (2006).
14. Du, K., Herzig, S., Kulkarni, R. N. & Montminy, M. TRB3: A *tribbles* homolog that inhibits Akt/PKB activation by insulin in liver. *Science* **300,** 1574–1577 (2003).
15. Okamoto, H. *et al.* Genetic deletion of Trb3, the mammalian *Drosophila* tribbles homolog, displays normal hepatic insulin signaling and glucose homeostasis. *Diabetes* **56,** 1350–1356 (2007).
16. Kohyama, M. *et al.* Role for Spi-C in the development of red pulp macrophages and splenic iron homeostasis. *Nature* **457,** 318–321 (2009).
17. De Domenico, I., McVey Ward, D. & Kaplan, J. Regulation of iron acquisition and storage: consequences for iron-linked disorders. *Nature Rev. Mol. Cell Biol.* **9,** 72–81 (2008).
18. Hong, S., Skaist, A. M., Wheelan, S. J. & Friedman, A. D. AP-1 protein induction during monopoiesis favors C/EBP: AP-1 heterodimers over C/EBP homodimerization and stimulates FosB transcription. *J. Leukoc. Biol.* **90,** 643–651 (2011).
19. Odegaard, J. I. & Chawla, A. Alternative macrophage activation and metabolism. *Annu. Rev. Pathol.* **6,** 275–297 (2011).
20. Lumeng, C. N., Bodzin, J. L. & Saltiel, A. R. Obesity induces a phenotypic switch in adipose tissue macrophage polarization. *J. Clin. Invest.* **117,** 175–184 (2007).
21. Odegaard, J. I. *et al.* Macrophage-specific PPARγ controls alternative activation and improves insulin resistance. *Nature* **447,** 1116–1120 (2007).
22. Reese, T. A. *et al.* Chitin induces accumulation in tissue of innate immune cells associated with allergy. *Nature* **447,** 92–96 (2007).
23. Satoh, T. *et al.* The Jmjd3-Irf4 axis regulates M2 macrophage polarization and host responses against helminth infection. *Nature Immunol.* **11,** 936–944 (2010).
24. Chawla, A., Nguyen, K. D. & Goh, Y. P. Macrophage-mediated inflammation in metabolic disease. *Nature Rev. Immunol.* **11,** 738–749 (2011).
25. Gregor, M. F. & Hotamisligil, G. S. Inflammatory mechanisms in obesity. *Annu. Rev. Immunol.* **29,** 415–445 (2011).
26. Hotamisligil, G. S. Inflammation and metabolic disorders. *Nature* **444,** 860–867 (2006).
27. Wellen, K. E. & Hotamisligil, G. S. Obesity-induced inflammatory changes in adipose tissue. *J. Clin. Invest.* **112,** 1785–1788 (2003).
28. Wu, D. *et al.* Eosinophils sustain adipose alternatively activated macrophages associated with glucose homeostasis. *Science* **332,** 243–247 (2011).
29. Odegaard, J. I. *et al.* Alternative M2 activation of Kupffer cells by PPARδ ameliorates obesity-induced insulin resistance. *Cell Metab.* **7,** 496–507 (2008).
30. Ricardo-Gonzalez, R. R. *et al.* IL-4/STAT6 immune axis regulates peripheral nutrient metabolism and insulin sensitivity. *Proc. Natl Acad. Sci. USA* **107,** 22617–22622 (2010).

Supplementary Information is available in the online version of the paper.

Acknowledgements We thank I. Shimomura and Y. Miyata for providing us with the key protocols for the metabolic experiments; T. Kitamura for providing the PlatE cells; M. Higa, H. Tanaka, N. Miyamoto, K. Miura, D. Ori, T. Uehata and K. Kuniyoshi for assistance with the experiments; and T. Kawai, S. Uematsu, T. Saitoh and Y. Kumagai for discussions. We also thank E. Kamada and M. Kageyama for secretarial assistance, and N. Umano, Y. Matsumoto and M. Kumagai for technical assistance. This work was supported by the Special Coordination Funds of the Japanese Ministry of Education, Culture, Sports, Science and Technology, and the Ministry of Health, Labour and Welfare in Japan, the Japan Society for the Promotion of Science through the Funding Program for World-Leading Innovative R&D on Science and Technology (FIRST Program).

Author Contributions T.S. designed and performed the experiments and wrote the manuscript. H.K., H.N. and N. Takakura performed the colony-forming assays. M.Y. generated the *Trib1*$^{-/-}$, *Trib2*$^{-/-}$ and *Trib3*$^{-/-}$ mice. N. Takemura helped with experiments. K.N. performed microarray analysis. Y.Y. performed the MRI experiments. E.M. performed the histological analyses. O.T. and S.A. designed experiments and wrote the manuscript. S.A. supervised the project.

Author Information Data have been deposited in the GEO under accession number GSE43563. Reprints and permissions information is available at www.nature.com/reprints. The authors declare no competing financial interests. Readers are welcome to comment on the online version of the paper. Correspondence and requests for materials should be addressed to S.A. (sakira@biken.osaka-u.ac.jp).